Cell. Mol. Life Sci. (2017) 74:339–358
DOI 10.1007/s00018-016-2337-4

Cellular and Molecular Life Sciences

ORIGINAL ARTICLE

Disruption of calcitonin gene-related peptide signaling accelerates muscle denervation and dampens cytotoxic neuroinflammation in SOD1 mutant mice

Cornelia Ringer[1,2] · Sarah Tune[3] · Mirjam A Bertoune[4] · Hans Schwarzbach[4] · Kazutake Tsujikawa[5] · Eberhard Weihe[1] · Burkhard Schütz[1]

Received: 28 January 2016 / Revised: 6 August 2016 / Accepted: 8 August 2016 / Published online: 23 August 2016

Abstract Amyotrophic lateral sclerosis (ALS) is a fatal motor neuron disease. Neuronal vacuolization and glial activation are pathologic hallmarks in the superoxide dismutase 1 (SOD1) mouse model of ALS. Previously, we found the neuropeptide calcitonin gene-related peptide (CGRP) associated with vacuolization and astrogliosis in the spinal cord of these mice. We now show that CGRP abundance positively correlated with the severity of astrogliosis, but not vacuolization, in several motor and non-motor areas throughout the brain. SOD1 mice harboring a genetic depletion of the βCGRP isoform showed reduced CGRP immunoreactivity associated with vacuolization, while motor functions, body weight, survival, and astrogliosis were not altered. When CGRP signaling was completely disrupted through genetic depletion of the CGRP receptor component, receptor activity-modifying protein 1 (RAMP1), hind limb muscle denervation, and loss of muscle performance were accelerated, while body weight and survival were not affected. Dampened neuroinflammation, i.e., reduced levels of astrogliosis in the brain stem already in the pre-symptomatic disease stage, and reduced microgliosis and lymphocyte infiltrations during the late disease phase were additional neuropathology features in these mice. On the molecular level, mRNA expression levels of brain-derived neurotrophic factor (BDNF) and those of the anti-inflammatory cytokine interleukin 6 (IL-6) were elevated, while those of several pro-inflammatory cytokines found reduced in the brain stem of RAMP1-deficient SOD1 mice at disease end stage. Our results thus identify an important, possibly dual role of CGRP in ALS pathogenesis.

Keywords Astrocyte · Chemokine · Microglia · Neuropeptide · Receptor activity-modifying protein 1 · Superoxide dismutase 1

Abbreviations

αBtx	Alpha-bungarotoxin
ACh	Acetylcholine
ALS	Amyotrophic lateral sclerosis
BDNF	Brain-derived neurotrophic factor
ChAT	Choline acetyltransferase
CD	Cluster of differentiation
CGRP	Calcitonin gene-related peptide
CLR	Calcitonin receptor-like receptor
GDNF	Glial cell line-derived neurotrophic factor
GFAP	Glial fibrillary acidic protein
Iba1	Ionized calcium-binding adapter molecule 1

Electronic supplementary material The online version of this article (doi:10.1007/s00018-016-2337-4) contains supplementary material, which is available to authorized users.

✉ Eberhard Weihe
weihe@staff.uni-marburg.de

✉ Burkhard Schütz
schuetzb@staff.uni-marburg.de

[1] Department of Molecular Neurosciences, Institute of Anatomy and Cell Biology, Philipps-University, Robert-Koch-Strasse 8, 35037 Marburg, Germany

[2] Institute of Anatomy, University of Lübeck, Lübeck, Germany

[3] Department of Physiology, University of Lübeck, Lübeck, Germany

[4] Department of Medical Cell Biology, Institute of Anatomy and Cell Biology, Philipps-University, Marburg, Germany

[5] Laboratory of Molecular and Cellular Physiology, Graduate School of Pharmaceutical Sciences, Osaka University, Yamadaoka, Suita, Osaka, Japan

IL	Interleukin
ir	Immunoreactivity
NMJ	Neuromuscular junction
P	Postnatal day
PaGE	Paw grip endurance test
RAMP1	Receptor activity-modifying protein 1
RCP	Receptor component protein
RT-PCR	Reverse transcriptase polymerase chain reaction
SOD1	Superoxide dismutase 1
TGF	Transforming growth factor
TNF	Tumor necrosis factor
VAChT	Vesicular acetylcholine transporter
VEGF	Vascular endothelial growth factor
VH	Ventral horn
WT	Wildtype
XII	Hypoglossal nucleus
Ywhaz	Tyrosine 3-monooxygenase/tryptophan 5-monooxygenase activation protein, zeta polypeptide

Introduction

Amyotrophic lateral sclerosis (ALS) is an adult-onset and lethal neurodegenerative disease. Progressive loss of motor neurons in cortex, brain stem, and spinal cord leads to denervation of skeletal muscles, paralysis, and ultimately death by respiratory failure. While 90 % of ALS cases occur sporadically, 10 % are inherited [1–3]. A recent comparative analysis of brain tissue led to the suggestion that ALS is a multi-system-disorder, rather than a pure motor neuron disease, because it shares pathological features with other brain disorders, such as fronto-temporal dementia [4]. Several variants of human ALS-triggering mutations have been used to establish transgenic mouse models that mimic human clinical symptoms and histopathological changes [5, 6]. In the superoxide dismutase 1 strain carrying a glycine to alanine mutation at position 93 ($SOD1^{G93A}$; abbrev. SOD1 throughout the report) [7], overt motor dysfunctions start around postnatal day (P) 90, and death occurs around P130. At the cellular level, a vacuolization pathology, i.e., vacuolization of motor neuronal mitochondria, is already detectable at the early pre-symptomatic stages between P30 and P40 [8, 9]. Subsequently, denervation of skeletal muscles occurs at P50 [10, 11], followed by changes in the morphology and number of astrocytes (astrogliosis) and microglia (microgliosis) [12, 13], and infiltration of lymphocytes [14, 15] at around P60. While the presence of human SOD1 immunoreactivity (ir) at the rim of the vacuolized mitochondria has been known for a long time [9], we found these structures to be immunoreactive for calcitonin gene-related peptide (CGRP) as well [16].

CGRP is a 37 amino acids long neuropeptide with two isoforms, αCGRP and βCGRP, that are co-expressed by motor and many other neuron types [17, 18]. The CGRP receptor trimer consists of the G-protein coupled calcitonin receptor-like receptor (CLR), a receptor component protein (RCP), and the receptor activity-modifying protein 1 (RAMP1) [19, 20], which confers ligand-specificity, and is expressed by both astrocytes and microglia [21–23]. CGRP expression in neurons is induced or up-regulated following, e.g., axotomy, inflammation or virus infection [24–28], and CGRP signaling on astroglia and microglia leads to cell activation [29–31]. Accordingly, CGRP is considered a signal of neuronal damage, secreted to induce repair mechanisms and supportive glial reactions [32].

Previously, we reported the presence of a close spatio-temporal association between CGRP-containing dysmorphic motor neuronal dendrites and processes of activated astrocytes in the lumbar spinal cord of pre-symptomatic SOD1 mice [33]. We also found that motor neurons without CGRP expression in brain stem nuclei did not show ALS pathology, and that higher motor neuron degeneration corresponded with higher levels of CGRP expression [34]. Notably, αCGRP was found to be the dominant isoform associated with motor neuron vulnerability, while βCGRP was the dominant isoform present at the rims of pathologic vacuoles and suggested to be associated with astrogliosis. A depletion of αCGRP in SOD1 mice, however, was not associated with a clinical or histopathological phenotype, suggesting that the other CGRP isoform compensated this loss.

To further delineate the potential importance of CGRP for the severity of vacuolization and/or astrogliosis during ALS pathogenesis in SOD1 mice, we now investigated if the abundance of CGRP positively correlated with vacuolization and/or astrogliosis throughout the brain, including areas beyond the somatomotor system; and if clinical outcome and histopathology were altered in SOD1 mice carrying a genetic depletion of either βCGRP, or RAMP1 [21].

Materials and methods

Mouse strains

SOD1

Transgenic mice of the strain B6SJL-TgN(SOD1(-G93A))1Gur (The Jackson Laboratory, Bar Harbor, ME)-carrying human SOD1 with the pathogenic G93A mutation ($SOD1^{G93A}$ (G1H)) in high copy number [35] were used as

animal model for ALS. The genotypes of mice were determined by PCR with established protocols [16], using genomic DNA obtained from ear punch biopsies. Wild-type (WT) littermates from breeding of SOD1 males with non-transgenic females were taken as controls where applicable, instead of using a WT-SOD1 overexpressing mouse line. While few of these WT-SOD1 mouse lines [9] show pathology features that are similar to those seen in the ALS-causing $SOD1^{G93A}$ mouse line, e.g., vacuolization and gliosis, and, hence, are valuable controls for some experiments, vacuolization in these mice appears not until P210, an age $SOD1^{G93A}$ mice do not reach. Thus, direct comparisons between the two lines on a histological level are not possible, which is why we consider a WT-SOD1 overexpressing mouse line not superior to WT littermates from our colony.

Calcb

Mice with a targeted loss-of-function mutation in the βCGRP-encoding gene were obtained from the Texas A&M Institute for Genomic Medicine (Houston, TX, USA; internal ref. no. TG0114). In these mice, exons 2–4 were replaced by a Bgeo/Puro cassette using a pKOS-40-targeting vector. Southern blot analysis identified several clones with a targeted allele, with at least one clone (1A9) achieving germline transmission. βCGRP−/− mice were obtained from breeding of βCGRP+/− mice. Mice were genotyped as described above. The mutant locus was amplified with primers TG0114-26: TAC TGC ACG TTT TGA GAG CTG CAG TG and GT-IRES: CCC TAG GAA TGC TCG TCA AGA, which resulted in a 346 bp amplicon. As a control, the WT locus was amplified with primers TG0114-13: TTT AAC CTG CTG ACT GCC GTA AGA and TG0114-14: GGG CCA CTG ATT CTC CGA CA, which resulted in a 402 bp amplicon.

Ramp1

Mice with a targeted loss-of-function mutation in the RAMP1-encoding gene were described earlier [36]. Mice were genotyped by PCR as described above using an established protocol [36].

All three mouse lines were backcrossed onto a C57BL/6 N inbred genetic background over at least 10 generations before use.

Double transgenic mice

Male SOD1 mice were mated with female βCGRP−/− (or RAMP1−/−) mice. Within the offspring WT:βCGRP+/− (RAMP1+/−), females were mated with SOD1:βCGRP+/− (RAMP1+/−) males, which resulted in the generation of six genotypes in the expected Mendelian frequency from which four genotypes were used for experimental analysis: WT:βCGRP+/+ (RAMP1+/+) = WT control group, WT:βCGRP−/− (RAMP1−/−) = βCGRP−/− (RAMP1−/−) control group, SOD1:βCGRP+/+ (RAMP1+/+) = SOD1 control group, and SOD1:βCGRP−/− (RAMP1−/−) = test group. In addition to these newly generated double transgenic mice, tissue from previously generated SOD1 mice with a genetic depletion of the *calca* gene, which codes for the αCGRP isoform, were used (28).

All mice were housed on a 12 h dark/light cycle in groups of two-to-four animals per cage with unrestricted access to food and water. From the time, mice carrying the SOD1 mutation showed motor deficits, additional moisturized food was placed on the cage floor. Because of ethical considerations, transgenic animals were sacrificed when their weight dropped below 80 % of the peak body weight. All animal procedures were conducted in accordance with the international standards on animal welfare, EU directive 2010/63/EU for animal experiments, the German Animal Protection Law, and animal protocols approved by the county administrative government (Gießen, Germany; no. 48/2010 for RAMP1, and 19/2013 for βCGRP). Adequate measures were taken to minimize pain or discomfort.

Determination of disease progression and motor functions

Starting at P49, the motor performances of all mice were assessed weekly with the paw grip endurance (PaGE) test that targets hind limb function [16, 37], and a licking test that targets tongue motor function [38, 39]. For PaGE testing, the mice were placed individually on a meshed wire platform, arranged rotatable about 60 cm above the bench. After the animal found a grip, the platform was gently turned upside-down and the latency recorded until the animal let loose with both hind legs. Each mouse was given a maximum of three consecutive trials to reach the cut-off time of 120 s, and the longest latency was recorded. To determine tongue motor function via the lick frequency during drinking, mice were placed in a cage equipped with a metal floor and water bottle with a metal spout, both connected to an analog/digital converter. Each lick of the mouse closed the current circuit, thereby inducing a minimal, non-perceptible voltage peak that was recorded by the converter and conferred on a computer. The average time difference between 25 consecutive peaks (=tongue licks) was calculated as lick frequency in Hertz (Hz). Body weight and survival time were monitored as additional parameters for disease progression. Determined, weekly, body weight was recorded as percentage of the weight at

the beginning of the study period (P49) to account for absolute weight differences between individual mice. All clinical parameters are given as mean with standard error of the mean (SEM). Survival times and time of PaGE onset are presented by a Kaplan–Meier plot and compared by Log-rank testing. The other clinical data were examined for statistical significance using the one-way ANOVA followed by Bonferroni corrected pair-wise comparisons.

Tissue processing

Mice were sedated by an overdose of inhaled isoflurane and, subsequently, killed by cervical dislocation (βCGRP study) or pneumothorax (RAMP1 study). L3–L5 segments of spinal cord and the quadriceps muscle were dissected and frozen in −40 °C cold isopentane. Fourteen micrometer-thick sections were cut with a cryotome and mounted onto silanized glass slides prior to fixation with 4 % (w/v) paraformaldehyde. Additional lumbar spinal cord segments and whole brains were immersion-fixed for 48 h in Bouin Hollande fixative, containing 4 % (w/v) picric acid, 2.5 % (w/v) cupric acetate, 3.7 % (v/v) formaldehyde, and 1 % (v/v) glacial acetic acid. Following fixation, the tissues were extensively washed in 70 % isopropanol, dehydrated, cleared with xylene, and embedded in paraffin. 7 µm-thick sections were cut with a microtome and mounted onto silanized glass slides. Histological counter stains were done by Giemsa staining. Finally, brain stem halves were dissected, submerged in RNAlater (LifeTechnologies, Darmstadt, Germany), and stored at 4 °C.

In situ hybridization

The generation of complementary RNA probes for the detection of mouse *calca* (αCGRP) and *calcb* (βCGRP) transcripts in tissue sections has been described previously [33]. The in situ-hybridization (ISH) procedure was performed on 20 µm cryostat sections as described in detail earlier [40]. Briefly, for pre-treatment, sections were air dried for 15 min, fixed in freshly prepared 4 % (w/v) paraformaldehyde in PBS for 60 min at room temperature and washed 3× for 10 min in 10 mM PBS. After a brief wash in distilled water, sections were acetylated with triethanolamine/acetic anhydride for 10 min at room temperature, followed by a 5 min wash in distilled water. The sections were then dehydrated through a graded series of isopropanol (50, 80, 96, 100 %; each 2 min), air dried for 30 min, and either directly used for hybridization or stored at −20 °C until use.

For hybridization, sections were covered with 30–40 µl of hybridization solution, containing 50 % formamide, 0.6 M NaCl, 10 mM Tris (pH 7.4), 1 mM Na_2EDTA, 1× Denhardts, 10 % dextran sulfate, 100 µg/ml sheared salmon sperm DNA, 0.05 % (w/v) *E. coli* MRE600 tRNA, 20 mM dithiothreitol, and 50,000 d.p.m./µl riboprobe and coverslipped. Hybridization was carried out overnight at 60 °C in a humid chamber. After hybridization, coverslips were removed in 2 × SSC at room temperature and the sections washed in the following order: 20 min in 1 × SSC, 45 min at 37 °C in RNase solution containing 20 µg/ml RNase A and 1 U/ml RNase T1, 20 min in 1 × SSC, 20 min in 0.5 × SSC, 20 min in 0.2 × SSC, 60 min in 0.2 × SSC at 60 °C, 10 min in 0.2 × SSC at room temperature, and 10 min in distilled water. Finally, sections were dehydrated in 50 and 70 % isopropanol and air dried at room temperature. For visualization of hybridization signals, sections were first exposed to Amersham β-Max autoradiography film for 1 to 3 days to estimate further exposure times, then coated with Kodak NTB2 emulsion, exposed for 21 days at 4 °C and developed. Sections were counterstained with cresyl violet, dehydrated through a graded series of isopropanol, cleared in xylene, and, finally, mounted under coverslips. Bright and dark field analysis was performed using an Olympus AX70 microscope (Olympus Optical, Hamburg, Germany).

Single immunohistochemistry

Tissue sections were deparaffinized in xylene and rehydrated through a graded series of isopropanol, including 30 min incubation in methanol/0.3 % H_2O_2 to block endogenous peroxidase activity. Antigen retrieval was achieved by incubation in 10 mM sodium citrate buffer (pH 6.0) at 92–95 °C for 15 min, and non-specific binding sites were blocked with 5 % bovine serum albumin (BSA) in 50 mM phosphate buffered saline (PBS, pH 7.45) for 30 min, followed by an avidin–biotin blocking step (Avidin–Biotin Blocking Kit, Boehringer, Ingelheim, Germany) for 20 min each. Primary antibodies were rabbit-anti-CGRP (1:200.000; Dr. Nyberg, Uppsala, Sweden), goat-anti-SOD1 (order no. sc-8637, final dilution 1:1.000; Santa Cruz Biotech., Heidelberg, Germany), goat-anti-ChAT (AB144P, 1:500; Chemicon, Hofheim, Germany), guinea pig-anti-GFAP (GP52, 1:5.000; Progen, Heidelberg, Germany), rabbit-anti-Iba1 (019-19741, 1:2.500; Wako Chemicals, Neuss, Germany), and rabbit-anti-CD3 (MCA1477, 1:3.000; DAKO, Hamburg, Germany), and applied in PBS/1 % BSA over night at 16 °C followed by 2 h at 37 °C. After several washes in PBS, the sections were incubated for 45 min at 37 °C with species-specific biotinylated secondary antibodies (Dianova, Hamburg, Germany), diluted 1:200 in PBS/1 % BSA, washed again, and, subsequently, incubated for 30 min with avidin–biotin–peroxidase complex (Vectastain Elite ABC kit; Vector Laboratories, Burlingame, CA). Immunoreactions were visualized by 8 min incubation in 3,3-diaminobenzidine (DAB, Sigma Aldrich, Deisenhofen,

Germany), enhanced by the addition of 0.08 % ammonium nickel sulfate (Fluka, Bucks, Switzerland). After three 5 min washes in distilled water, the sections were dehydrated through a graded series of isopropanol, cleared in xylene, and, finally, mounted under coverslips. Digital bright-field pictures were taken with an Olympus AX70 microscope (Olympus Optical, Hamburg, Germany), equipped with a SPOT RT Slider Camera and SPOT Image Analyses software (Version 3.4; Diagnostic Instruments Inc., Seoul, Korea).

Double immunofluorescence

To assess the association of astrocyte activation with vacuolization, standard double immunofluorescence was performed on paraffin sections as follows: After deparaffination and blocking procedures (see above), goat-anti-SOD1 (1:500) and either guinea pig-anti-GFAP (1:2.000), or rabbit-anti-CGRP (1:10.000) primary antibodies were co-applied in PBS/1 % BSA and incubated overnight at 4 °C, followed by 2 h at 37 °C. After extensive washing in distilled water followed by PBS, SOD1 immunoreactions were visualized with anti-goat secondary antibodies labeled with Alexa Fluor 647 (MoBiTec, Göttingen, Germany), diluted 1:200 in 1 % BSA/PBS. The GFAP and CGRP antibodies were visualized, respectively, by a two-step procedure, including species-specific biotinylated secondary antibody (Dianova), diluted 1:200 in 1 % BSA/PBS followed by streptavidin conjugated with Alexa Fluor 488, diluted 1:200 in 1 % BSA/PBS. Incubation times were 45 min with the biotinylated secondary antibody only, followed by 2 h incubation with a mixture of fluorochrome-conjugated secondary antibody and streptavidin.

A modified histo- and immuno-fluorescence procedure was applied for the detection of neuromuscular endplates using α-bungarotoxin (αBtx): Paraformaldehyde-fixed cryostat sections of muscle tissue were processed without antigen retrieval. Following the blocking steps, a rabbit-anti-vesicular acetylcholine transporter antibody (VAChT, 1:5.000; Dr. Eiden, Bethesda, USA) was used in combination with αBtx (Invitrogen, Eugene, USA) conjugated with Alexa Fluor 647, to label the post-synaptic acetylcholine receptors on muscle fibers. VAChT binding was visualized with an anti-rabbit secondary antibody conjugated with Alexa-488 (1:200, Dianova). Incubation times and washing steps were analog to the standard double immunofluorescence described above.

Immunofluorescence signals were documented as digitized false color images (8-bit tiff format) with an Olympus BX50WI confocal laser scanning microscope (Olympus Optical, Hamburg, Germany) and Olympus Fluoview 2.1 software without modifications in brightness and contrast.

Quantitative assessment of histopathology

For each aspect investigated, four animals per genotype and age, and five sections per animal were analyzed. To assess correlations between CGRP abundance, pathologic vacuolization, and astrogliosis, sagittal brain sections stained with single immunohistochemistry against CGRP, SOD1, and GFAP were digitized using a Leica CTR 6500 microscope equipped with Metamorph Leica MMAF (Version 1.4.0.) and a Leica DCF310 FX camera. Whole sections were scanned in frames with tenfold optic magnification (numerical aperture = 0.4) and assembled by seamless multichannel rendering to 100 megapixel images, with a resulting resolution of 1 µm/pixel. The scans were displayed in zoomify Web pyramid image format, coordinates for the different regions of interest (see Table 1) were set, and images extracted as jpeg using Python/PIL and Numpy.

To quantify the immunoreactivities of CGRP, SOD1, and GFAP, the images were analyzed with Image J (National Institutes of Health, Bethesda, Maryland, USA) by setting a constant threshold of optic density. All immunoreactions above threshold were gathered and given as percentage immunoreactive area. Data values are given as mean with standard error of the mean (SEM), and analyzed with Kruskal–Wallis one-way analysis of variance by ranks followed by Bonferroni corrected pair-wise comparisons, and by calculation of Pearson's correlation coefficient. p values less than 0.05 were regarded as significant.

For quantitative assessment of neurodegeneration, motor neurons labeled by ChAT-ir were counted manually, including only soma with clearly cut and healthy looking (round) nucleus to exclude neurons in degeneration. In addition, multiple sections from a single tissue were 21 µm apart to avoid double counting of neurons.

To assess muscle denervation, αBtx-labeled neuromuscular endplates with and without associated VAChT-immunoreactivity were counted manually. Sections were 14 µm apart to avoid double counting.

Quantification of neuroinflammation was performed as previously described [41]. Briefly, images from bright-field staining against GFAP (astrocytes), Iba1 (microglia), and CD3 (lymphocytes) were acquired with MCID Elite™ 7.0 software (Imaging Research Inc., St. Catherines, Canada) and analyzed with ImageJ. In the area of interest, i.e., the lateral aspect of the ventral horn grey matter [8] and the para-medial brain stem, immunoreactive structures were determined by setting a constant threshold of optic density. All immunoreactions above threshold were gathered and given as percentage immunoreactive area for astrocytes and as number of immunoreactive particles (at least 20 connected pixels) per area for microglia and lymphocytes,

Table 1 Brain regions selected for histopathology analysis

Abbr.	Region	CGRP*	SOD1*	Function	Area (μm^2)
IntP	Interposed cerebellar nucleus	?	++	Extrapyramidal motor system	400
RN	Red nucleus	?	++	Extrapyramidal motor system	200
SNC	Substantia nigra pars compacta	?	+++	Extrapyramidal motor system	1600
LC	Locus coeruleus	?	+++	Other/multifunctional	1600
AD	Anterodorsal thalamic nucleus	?	+++	Other/multifunctional	400
HDB	Horizontal diagonal band	?	++	Other/multifunctional	400
Hc	Hippocampus	?	++	Other/multifunctional	1600
Hyp	Hyopthalamus	?	+	Other/multifunctional	2500
VII	Facial nucleus	+++	+++	Pyramidal motor system	1600
FF	Field of forel	++	?	Other/multifunctional	400
LS	Lateral septal nucleus	+++	?	Other/multifunctional	900
SolT	Solitary tract	+++	?	Sensory system	400
EPL	External plexiform layer of olfactory bulb	+	?	Sensory system	200
GrO	Granular layer of the olfactory bulb	0	?	Sensory system	200
Thal	Thalamus	0	0	Other/multifunctional	6400
M1/2	Primary and secondary motor cortices	?	?	Pyramidal motor system	6400
CPu	Caudate nucleus and putamen (striatum)	?	?	Extrapyramidal motor system	2500

Abbr., abbreviation of region name; CGRP*, selection criterion = CGRP abundance in cell bodies and/or fibers (subjective estimation), determined in P120 WT mice; SOD1*, selection criterion = severity of SOD1-positive vacuolization (subjective estimation), determined in end stage SOD1 animals; +++, high; ++, medium; +, low; 0, non; ?, to be determined

respectively. These data were analyzed with Kruskal–Wallis one-way analysis of variance followed by Bonferroni corrected pair-wise comparisons. p values less than 0.05 were regarded as significant.

Gene expression analysis by quantitative RT-PCR

Messenger RNA expression levels were measured by quantitative real-time PCR (qPCR) using the ABI PRISM® 7900HT System (Applied Biosystems, Foster City, CA, USA). First, tissue samples were mechanically disrupted in a PreCellys 24 homogenizer (PeqLab, Erlangen, Germany) for 2 × 20 s at 5.000 rpm. Total RNA was then extracted using the RNeasy Mini Kit® (Qiagen, Hilden, Germany), its degree of purity and integrity analyzed by the Experion™ automated gel electrophoresis system (Bio Rad Laboratories GmbH, Munich, Germany), and RNA quantity determined using a Nanodrop 2000c spectrophotometer (Peqlab). 800 ng of total RNA with a 260/280 nm ratio of 1.9–2.1 and a 260/230 nm ratio of 1.8–2.0 were translated into cDNA using the RT^2 HT First Strand Kit (Qiagen) according to the manufacturer's instructions. This included a non-RT reaction for each sample to check for genomic DNA contamination. For all subsequent PCR reactions, gene-specific QuantiTect primer pairs (Qiagen) were used to detect transcripts of *Actb* (GenBank NM_007393, order no. QT00095242), *arginase-1* (NM_007482, QT00134288), *BDNF* (NM_007540, QT00097118), *CCl2* (NM_011333, QT00167832), *CCL3* (NM_011337, QT00248199), *CCL5* (NM_013653, QT01747165), *CD68* (NM_009853, QT00254051), *CXCL10* (NM_021274, QT00093436), *GDNF* (NM_010275, QT00115290), *IGF-1* (NM_001111274, QT00154469), *Il-1β* (NM_008361, QT01048355), *Il-6* (NM_031168, QT00098875), *NOS2* (NM_010927, QT00100275), *TGFβ* (NM_011577, QT00145250), *TNFα* (NM_013693, QT00104006), *VEGF* (NM_001025250, QT00160769), *Ym1 (Chil3)* (NM_009892, QT00108829), and *Ywhaz* (NM_011740, QT00105350). Each PCR reaction consisted of 12.5 µl Power SYBR Green PCR Master Mix (Applied Biosystems), 2.5 µl gene-specific primer pair, 1 µl cDNA, and 9 µl H_2O, and was performed with RT^2 *Profiler*™ PCR Array 96-well plates (Qiagen). Amplification conditions were: 95 °C for 10 min, followed by 35 cycles at 95 °C for 15 s, and 60 °C for 30 s. A dissociation curve analysis confirmed the amplification of a single band. In addition, each cDNA underwent a mouse genomic DNA contamination and a reverse transcription control. Fluorescence signals were normalized to the passive internal reference dye, ROX, and a threshold (C_T) set within the first half of the exponential phase of the reaction. After calculating the mean value from triplicate reactions, relative abundances of transcripts in a given sample were first calculated as differences in C_T compared with the geomean of two independent housekeeping genes, *Actinb* and *Ywhaz* (ΔC_T), and then relative to WT ($\Delta\Delta C_T$). GraphPad Prism 6.0

(GraphPad Software Inc., La Jolla, CA, USA) was used for layout and statistical testing. Data from 3 to 5 samples per genotype and age were averaged and analyzed by one-way ANOVA followed by Bonferroni correction. For all analyses, a p value <0.05 was considered significant.

Results

Spatio-temporal correlations of CGRP abundance with vacuolization and with astrogliosis in motor and non-motor areas throughout the brain of SOD1 mice

Previously, we had observed a close spatio-temporal association of CGRP-immunoreactive vacuoles with astrogliosis in the spinal cord of SOD1 mice [33]. The appearance and morphological dynamics of CGRP-ir vacuolization were found also to be true for ALS-vulnerable motor nuclei in the brain stem (Suppl. A). However, because both, vacuolization and astrogliosis, develop throughout the brain in SOD1 mice [42, 43], we now quantified the level of vacuolization and astrogliosis in 18 brain areas (see Table 1) at two disease stages (early: P40/P60, and late: P120/end stage; see Suppl. C), and asked if CGRP abundance in the affected brain areas correlated with the severity of these neuropathologic hallmarks. Single and double immunohistochemical analyses using GFAP as a marker for astrocytes and SOD1 for ALS-related vacuoles revealed varying degrees of astrogliosis compared with the level of vacuolization throughout the brain. For example, in the anterodorsal nucleus of the thalamus (AD) and in the substantia nigra (SNC), two nuclei being densely vacuolated, no prominent astrogliosis was found in SOD1 end-stage mice compared with WT (Fig. 1A and Suppl. B). In contrast, less pronounced vacuolization of, e.g., the red nucleus (RN) and the locus coeruleus (LC) was accompanied with strong astrogliosis (Fig. 1A and Suppl. B). Interestingly, we found CGRP-immunoreactive fibers present in WT mice in regions with strong glial activation, but largely absent in regions with weak glial activation (e.g., AD and RN, Fig. 1A). To test if CGRP abundance positively correlated with astrogliosis and vacuolization throughout all regions investigated, we performed a comparative analysis of GFAP- and SOD1-ir with CGRP (Suppl. C). While the correlation analysis between CGRP abundance and vacuolization did not reach significance (Pearsons correlation coefficient $r = 0.48$ for P40 and $r = 0.49$ for end stage, Fig. 1C, panel a + b), a positive correlation was detected between CGRP abundance and astrogliosis at both disease stages ($r = 0.59$ for P60, $p = 0.01$; $r = 0.62$ for end stage, $p = 0.006$; Fig. 1B, panel a + b). In addition, the increase of GFAP-ir from early disease stage to end stage correlated with CGRP abundance ($r = 0.56$, $p = 0.015$) as well, whereas the increase of SOD1-ir was neither significantly correlated with CGRP abundance in WT ($r = 0.44$: Fig. 1B, panel c), nor with the increase of GFAP-ir SOD1 mice ($r = 0.48$, not shown).

Taken together, these data demonstrate a clear positive correlation of CGRP abundance and the severity of astrogliosis. This indicates an involvement of CGRP in ALS-related neuroinflammation that is independent of the SOD1 mutation and, thus, the overexpression of either wild-type or mutated SOD1.

Outcome of a genetic depletion of βCGRP in SOD1 mice

One of our previous studies suggested that CGRP immunoreactivity at the rim of the pathologic vacuoles was mainly attributable to the βCGRP isoform, because the genetic depletion of αCGRP had no effect on CGRP immunoreactivity in vacuolization or on astrogliosis in SOD1 mice [33]. We now benefited from the generation of a βCGRP-deficient mouse strain and were able to cross-breed these mice with the SOD1 strain. The βCGRP-deficient mice were born with the expected Mendelian frequency. They did not show any obvious phenotype, developed normally, and were fertile. Successful disruption of the βCGRP gene locus was proven by the absence of βCGRP-specific mRNA using ISH. Shown for the lumbar spinal cord, motor neurons still expressed αCGRP, but signals for βCGRP-mRNA were absent (Fig. 2A). After successfully obtaining SOD1:βCGRP−/− mice, we found CGRP-ir at the rims of the vacuoles in the ventral horn to be largely reduced compared with SOD1:αCGRP−/− and SOD1:WT mice (Fig. 2B). On the other hand, CGRP-ir in sensory fibers in the dorsal horn of SOD1: βCGRP−/− mice was similar to WT, but reduced in SOD1:αCGRP−/− mice. These results show that CGRP-ir in soma and neurites of motor (and sensory) neurons are mostly based on the α-isoform [34], while the pathological immunoreactivity related to vacuolization is derived from mislocalization of βCGRP [33].

At the clinical level, disease progression in SOD1:βCGRP−/− mice was found unaltered compared with SOD1:βCGRP+/+ mice (Fig. 2C). Median survival was determined to be 140 days for SOD1:βCGRP−/− and 141 days for SOD1:βCGRP+/+ mice (p = n.s.). All four study groups showed a comparable, initial increase in body weight. While WT ($n = 19$) and βCGRP−/− ($n = 12$) mice constantly gained weight over time, SOD1:βCGRP+/+ ($n = 18$) and SOD1:βCGRP−/− ($n = 18$) mice reached their maximum weight at around P80, and started to gradually lose weight thereafter. The SOD1:βCGRP+/+

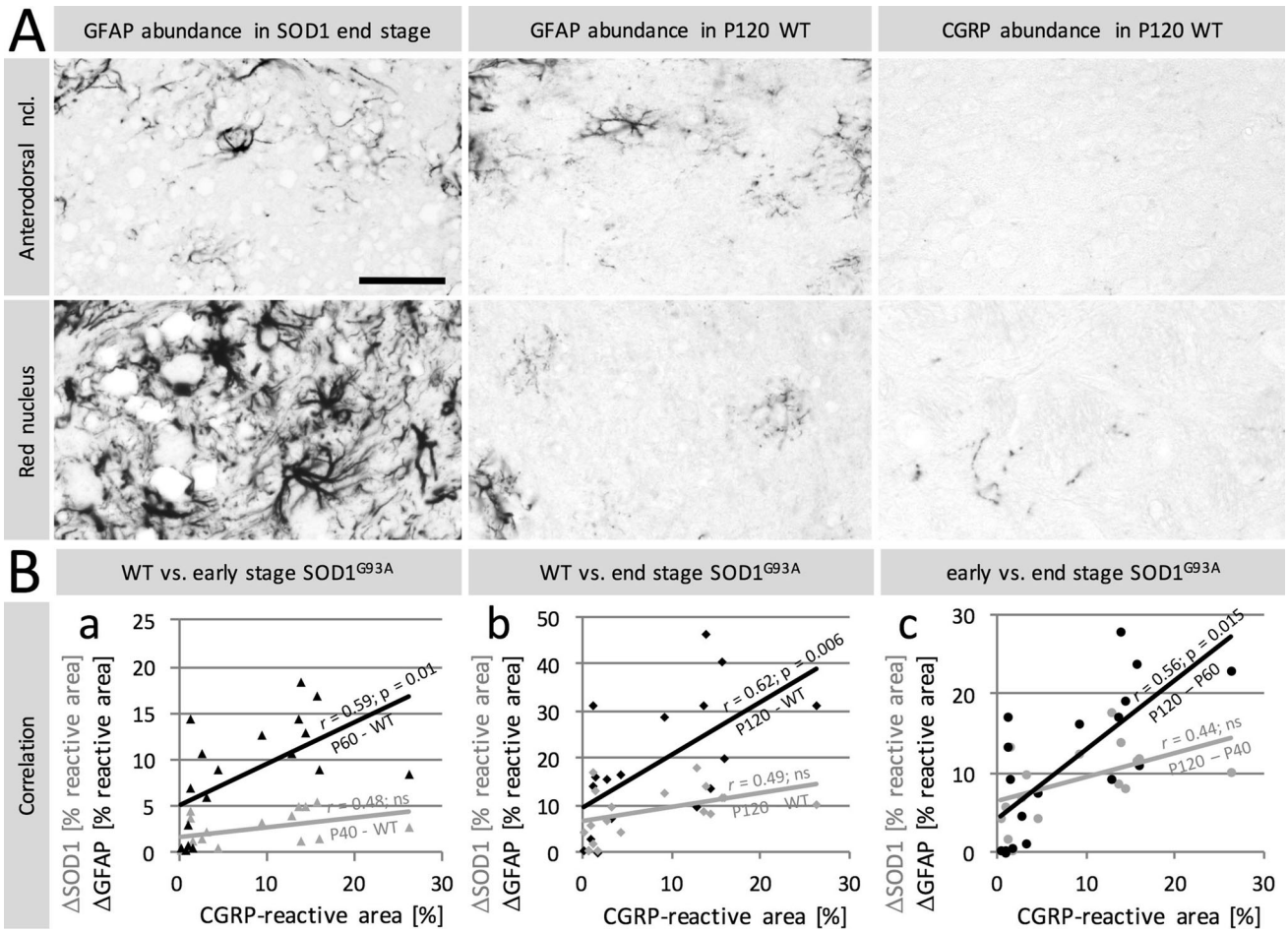

Fig. 1 Correlation analyses between SOD1-related vacuolization and astrogliosis with CGRP abundance. **A** CGRP abundance in WT mice in regions with strong and weak astrogliosis in SOD1 mice. Immunohistochemical analysis revealed a marginal increase of GFAP immunoreactivity (ir) in the anterodorsal nucleus of the thalamus (*upper panel*) in SOD1 end-stage mice (*left*) compared with WT (*middle*) as well as the absence of CGRP-immunoreactive fibers in WT (*right*). In contrast, in the red nucleus (*lower panel*), GFAP-ir in SOD1 mice (*left*) was found largely increased compared with WT (*middle*), and contained CGRP-immunoreactive fibers (*right*). *Bar* in **A** represents 50 μm and accounts for all pictures. **B** Correlation analysis between vacuolization and astrogliosis with CGRP abundance. Calculation of Pearson's correlation coefficient (*r*) of CGRP-abundance in WT with the increase of SOD1- and GFAP-ir (ΔSOD1 and ΔGFAP) in SOD1 mice compared with WT. *a* Comparison of WT with P40 (for SOD1) and P60 (for GFAP) SOD1 mice. *b* Comparison of WT with P120 (end stage) SOD1 mice. *c* Comparison of the increases of SOD1- and GFAP-ir between early and end-stage SOD1 mice

and SOD1:βCGRP−/− groups did not show a significant difference at any time point, and both genotypes were equally different from their respective control groups starting with P105 ($p < 0.05$). In the PaGE test, SOD1:βCGRP+/+ and SOD1:βCGRP−/− mice showed a very similar progressive decline in grip endurance, as well as a comparable decline in lick frequency of the tongue.

At the cellular level (Fig. 2D), no differences in motor neuron numbers or astrogliosis were present between end stage SOD1:βCGRP+/+ and SOD1:βCGRP−/−, neither in the lumbar spinal cord (corresponding to the tested hind limb motor function) nor in the brainstem (exemplified here for the hypoglossal nucleus corresponding to the tested tongue motor function).

Taken together, the absence of βCGRP in SOD1 mice largely reduced occurrence of CGRP-ir at the rims of pathologic vacuoles. However, clinical symptomatology and survival as well as neurodegeneration and astrogliosis remained unaltered when compared with WT, probably because the remaining αCGRP was sufficient to functionally compensate the depletion of βCGRP.

A RAMP1 deficiency accelerates disease onset and decelerates disease progression in SOD1 mice

Given the large overlap of αCGRP and βCGRP expression patterns and the high homology between the two isoforms, it seemed likely that one isoform substituted the function of

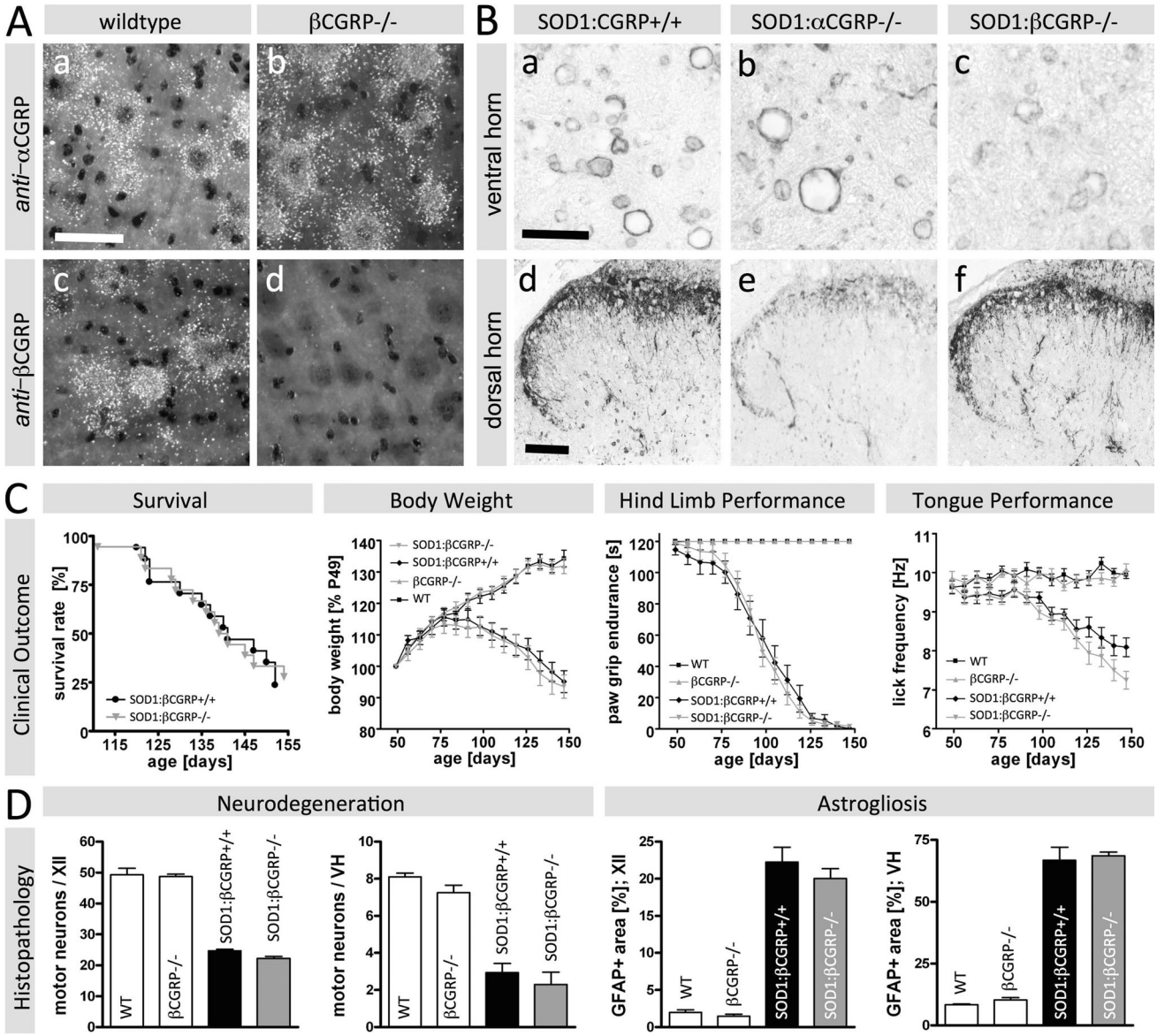

Fig. 2 Characterization of a βCGRP-deficient mouse strain and outcome of crossbreeding with SOD1 mice. **A** In situ-hybridization for the presence of αCGRP and βCGRP-mRNA in WT and βCGRP−/− mice. αCGRP-mRNA was detected in both WT and βCGRP−/− mice, while βCGRP-mRNA was detected in WT, but undetectable in βCGRP−/− mice. The *bar* equals 100 μm and accounts for all pictures. **B** CGRP-ir in lumbar spinal cord of end-stage SOD1 mice with and without CGRP isoform depletions. Note that in the ventral horn (*top*), CGRP-ir in SOD1-related vacuolization is similar in SOD1:CGRP+/+ (*a*) and SOD1:αCGRP−/− (*b*), but reduced in SOD1:βCGRP−/− mice (*c*). In contrast, CGRP-ir in sensory fibers in the dorsal horn (*bottom*) is reduced in SOD1:αCGRP−/− (*e*) but unaltered in SOD1:βCGRP−/− (*f*) compared with SOD1:CGRP+/+ (*d*). The *bar* in *a* equals 20 μm and also accounts for *b* and *c*; *bar* in *d* equals 100 μm and also accounts for *e*, *f*. **C** Clinical outcome of a βCGRP deficiency in SOD1 mice. Note that deficiency of βCGRP had no effect on survival, disease-related decline in body weight, and hind limb and tongue motor performances. **D** Histopathological outcome of a βCGRP deficiency in SOD1 mice. The number of motor neurons (MN) in hemi-sections of the hypoglossal nucleus (XII) and in the ventral horn of the lumbar spinal cord (VH) was reduced to about 50 and 30 %, respectively, until end stage in SOD1 mice, without differences between βCGRP-competent and -deficient littermates. GFAP-positive area, indicating activated astrocytes, was largely increased in both brain stem and spinal cord, without differences between βCGRP-competent and -deficient littermates

the other in a single knockout situation, which explains the lack of an overt phenotype in either αCGRP- or βCGRP-deficient SOD1 mice. Thus, a complete loss of CGRP signaling was needed to further elucidate the function of this neuropeptide in ALS pathology. Since both CGRP genes are located in close proximity on the same chromosome, a crossbreeding of αCGRP−/− and βCGRP−/− mice to obtain a panCGRP knockout seemed an impossible

strategy to further investigate the functional relevance of CGRP signaling as a whole in ALS mice. Therefore, we crossbred a *Ramp1*-deficient mouse line into SOD1 mice to completely perturb CGRP signaling.

At the clinical level, the median survival was assessed as 142 days for SOD1:RAMP1−/− mice and 137 days for SOD1:RAMP1+/+ mice (p = n.s., Fig. 3a). WT ($n = 10$) and RAMP1−/− ($n = 15$) mice constantly gained weight over time, while both SOD1:RAMP1+/+ ($n = 22$) and SOD1:RAMP1−/− ($n = 17$) mice reached their maximum weight at around P80, and started to gradually lose weight thereafter, without significant differences between the groups. However, during the period of weight gain, SOD1:RAMP1−/− mice differed significantly from RAMP1−/− already at P70, while SOD1:RAMP1+/+ did not differ from WT until they reached the peak at P91 (Fig. 3a). When tested for PaGE, 3 of the 17 SOD1:RAMP1−/− mice did not reach the 2 min cut-off time even during the first assessment at P49. Accordingly, the SOD1:RAMP1−/− group showed a significant reduction in the hind limb performance compared to RAMP1−/− as early as P49 (Fig. 3a). In contrast, the decline in hind limb motor performance in SOD1:RAMP1+/+ compared with WT mice reached significance only from P77 onward. Notably, the initial decline in hind limb performance in SOD1:RAMP1−/− mice did not further progress between P56 and P98, and both SOD1:RAMP1−/− and SOD1:RAMP1+/+ mice showed a similar and fast reduction of hind limb grip endurance from P105 until end stage. In contrast, tongue motor performance did not differ between SOD1:RAMP1−/− and SOD1:RAMP1+/+ groups at any analyzed time point. However, similar to body weight and hind limb weakness, SOD1:RAMP1−/− differed from RAMP1−/− earlier than SOD1:RAMP1+/+ from WT (P105 vs. P119, Fig. 3a).

Thus, SOD1:RAMP1−/− mice showed an accelerated symptom onset in all clinical parameters we assessed, although a significant difference to SOD1:RAMP1+/+ was only found for hind limb grip endurance. In addition, matching disease onset in individual mice based on hind limb symptoms (i.e., the time point, where the cut-off time in the PaGE was not reached anymore) instead of defining disease onset by comparing whole, age-matched groups revealed a change in the time course of symptom development between SOD1:RAMP1−/− and SOD1:RAMP1+/+ mice (Fig. 3b): Disease onset was found accelerated (P56.5 ± 30.4 in SOD1:RAMP1−/− vs. P92.0 ± 20.0 in SOD1:RAMP1+/+, $p < 0.001$, Fig. 3b, left panel), while disease duration was prolonged when compared with SOD1:RAMP1+/+ mice (85.7 ± 26.5 in SOD1:RAMP1−/− vs. 46.9 ± 22.3 days in SOD1:RAMP1+/+; $p < 0.001$; Fig. 3b, middle panel). Furthermore, the onset matching of individual mice revealed a continuous but decelerated decline of hind limb grip endurance in SOD1:RAMP1−/− compared with SOD1:RAMP1+/+ mice from 3 weeks after symptom onset until end stage (Fig. 3b, right panel).

Taken together, the RAMP1 deficiency resulted in an accelerated disease onset that was followed by a decelerated disease progression (Fig. 3b), and added up to an unaltered survival rate (Fig. 3a).

Fig. 3 Clinical and histopathological outcome of the RAMP1 depletion in SOD1 mice. **a** Clinical outcome. Deficiency of RAMP1 did not result in any significant differences in survival or on the disease-related decline in body weight and licking frequency of the tongue, but onset of hind limb weakness was accelerated. In addition, for all three clinical parameters, the symptom onset, i.e., the time point where SOD1 mice significantly differed from their respective control groups (indicated by *arrowheads*) was earlier for RAMP1−/− mice compared to their RAMP1+/+ littermates. **b** Disease development. Determination of hind limb grip endurance revealed that SOD1:RAMP1−/− mice showed an accelerated symptom onset and a prolonged disease duration compared with SOD1:RAMP1+/+ littermates. Matching individual mice by symptom onset instead of age revealed a continuous decline in hind limb grip endurance that was decelerated in SOD1:RAMP1−/− mice. **c** Neurodegeneration and muscle denervation. Motor neuron loss determined in hemi-sections of the hypoglossal nucleus (XII) and of the ventral horn (VH) of the lumbar spinal cord was similar in SOD1:RAMP1−/− and in SOD1:RAMP1+/+ mice. Combined histochemical (αBtx, Alexa 647-conjugated) and immuno-fluorescence (VAChT, Alexa 488-conjugated) discriminated innervated (VAChT-positive, *arrow*) and denervated (VAChT-negative, *arrowhead*) neuromuscular junctions (NMJ). **d** Neuroinflammation. Astrogliosis was significantly reduced in SOD1:RAMP1−/− mice compared with SOD1:RAMP1+/+ mice in all stages investigated. Microgliosis and infiltration of lymphocytes were similarly reduced in SOD1:RAMP1−/−, however, reaching significance only in the late stage of the disease at P120. *Ash* indicates differences to the corresponding RAMP1−/− or RAMP+/+ wild type (WT); and *asterisk* indicates differences between SOD1:RAMP1−/− and SOD1:RAMP1+/+ genotypes of the same age

The RAMP1 deficiency accelerates muscle denervation in SOD1 mice

Next, we assessed histopathological events that may account for the observed differences between SOD1 mice with and without CGRP signaling with respect to disease initiation and progression. While motor neuron degeneration in both the hypoglossal nucleus (XII, tongue innervation) and in the ventral horn of the lumbar spinal cord (hind limb innervation) followed a similar time course in SOD1:RAMP1+/+ and in SOD1:RAMP1−/− mice, muscle denervation initiated earlier in the latter (Fig. 3c). As determined by a combined histochemical and immunofluorescence against alpha-bungarotoxin (αBtx, labeling post-synaptic site of the NMJ) and the vesicular acetylcholine transporter (VAChT, labeling the pre-synaptic site of the NMJ), respectively, denervation of both tongue and

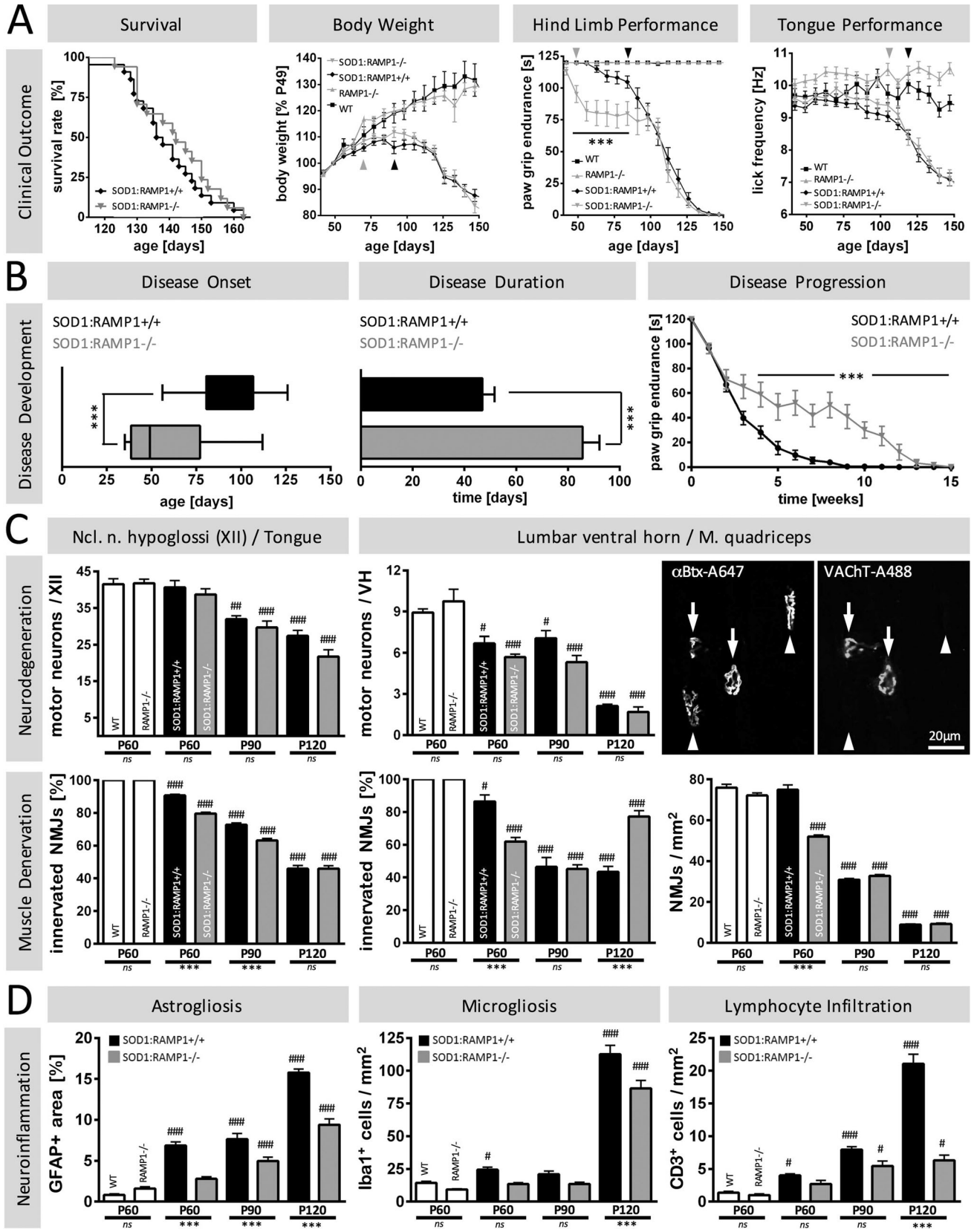
A
Survival
Body Weight
Hind Limb Performance
Tongue Performance
Clinical Outcome
survival rate [%]
age [days]
SOD1:RAMP1+/+
SOD1:RAMP1-/-
body weight [% P49]
SOD1:RAMP1-/-
SOD1:RAMP1+/+
RAMP1-/-
WT
paw grip endurance [s]
***
lick frequency [Hz]
B
Disease Onset
Disease Duration
Disease Progression
Disease Development
time [days]
time [weeks]
C
Ncl. n. hypoglossi (XII) / Tongue
Lumbar ventral horn / M. quadriceps
Neurodegeneration
motor neurons / XII
motor neurons / VH
αBtx-A647
VAChT-A488
20µm
Muscle Denervation
innervated NMJs [%]
NMJs / mm²
P60
P90
P120
ns
D
Astrogliosis
Microgliosis
Lymphocyte Infiltration
Neuroinflammation
GFAP+ area [%]
Iba1⁺ cells / mm²
CD3⁺ cells / mm²

quadriceps muscle neuromuscular junctions (NMJ) was already more pronounced at P60 for SOD1:RAMP1−/− compared with SOD1:RAMP1+/+ mice. In the tongue, the total number of NMJ (detected by αBtx staining) remained unchanged at around 120/mm^2 for both WT and RAMP1−/− as well as SOD1:RAMP1−/− and SOD1:RAMP1+/+ at P60 and P90, before dropping to about 80/mm^2 until end stage in both SOD1:RAMP1+/+ and SOD1:RAMP1−/− mice (not shown).

However, although no changes were detected in tongue motor performance, the proportion of innervated (αBxt- and VAChT-positive) NMJ at P60 and P90 was significantly higher in SOD1:RAMP1+/+, while in both genotypes, about half of the remaining NMJ were still innervated at end stage. In contrast, the proportion of innervated NMJ in the M. quadriceps was significantly lower at P60 (86.4 ± 4.0 % in SOD1:RAMP1+/+ vs. 61.9 ± 2.4 % in SOD1:RAMP1−/−, $p < 0.001$), similar at P90 (about 45 % each), and significantly higher at P120 (77.3 ± 3.5 % in SOD1:RAMP1−/− vs. 43.4 ± 3.5 % in SOD1:RAMP1+/+, $p < 0.001$). However, the total number of NMJ was equally reduced to about 10/mm^2 at disease end stage for both SOD1:RAMP1−/− and SOD1:RAMP1+/+ (Fig. 3c), meaning that in SOD1:RAMP1−/−, about 8 NMJ/mm^2 were still innervated, while in SOD1:RAMP1+/+, only about 4 functional NMJ/mm^2 remained at disease end stage. In contrast, at P60, the total number of NMJ was unaltered in SOD1:RAMP1+/+ (74.9 ± 2.3/mm^2) compared with WT (75.9 ± 1.6/mm^2), while already reduced in SOD1:RAMP1−/− (52.1 ± 0.7/mm^2) compared with RAMP1−/− (72.1 ± 1.6/mm^2, $p < 0.001$), resulting in a total of about 65 innervated (functional) NMJ/mm^2 in SOD1:RAMP1+/+ compared with only 32 innervated (functional) NMJ/mm^2 in SOD1:RAMP1−/−, which may explain the differences in hind limb motor performance in the early disease stages.

The RAMP1 deficiency dampens neuroinflammation and lymphocyte infiltration in SOD1 mice

Shown here for the brainstem (Fig. 3d), astrogliosis was significantly reduced in SOD1:RAMP1−/− mice when compared with SOD1:RAMP1+/+ mice at all stages investigated (P60: 6.9 ± 0.4 % vs. 2.8 ± 0.3 %, $p < 0.001$; P90: 7.6 ± 0.7 % vs. 4.9 ± 0.5 %, $p < 0.001$; P120: 15.8 ± 0.4 % vs. 9.4 ± 0.7 %, $p < 0.001$). Exemplified for hypothalamus (Fig. 4a–d) and red nucleus (Fig. 4e–h), this obvious reduction in astrogliosis in SOD1:RAMP1−/− mice was observed throughout the brain, suggesting that the correlation we found between CGRP abundance in WT and astrogliosis in SOD1 mice (Fig. 1C) was based on a functional relation.

Since the different cell types involved in neuroinflammation are known to influence each other via an extensive, cytokine-mediated crosstalk, we extended or investigations to microglia and lymphocytes: While microgliosis and infiltration of CD3-positive lymphocytes (i.e., T cells) started around P60 in SOD1:RAMP1+/+ mice (microglia: 14.5 ± 1.1 cells/mm^2 in WT vs. 24.5 ± 1.8 cells/mm^2 in SOD1:RAMP1+/+, $p < 0.05$; lymphocytes: 1.3 ± 0.2 cells/mm^2 in WT vs. 4.0 ± 0.3 cells/mm^2 in SOD1:RAMP1+/+; $p < 0.05$), no significant increase in Iba1- and CD3-positive cells was detected prior to disease

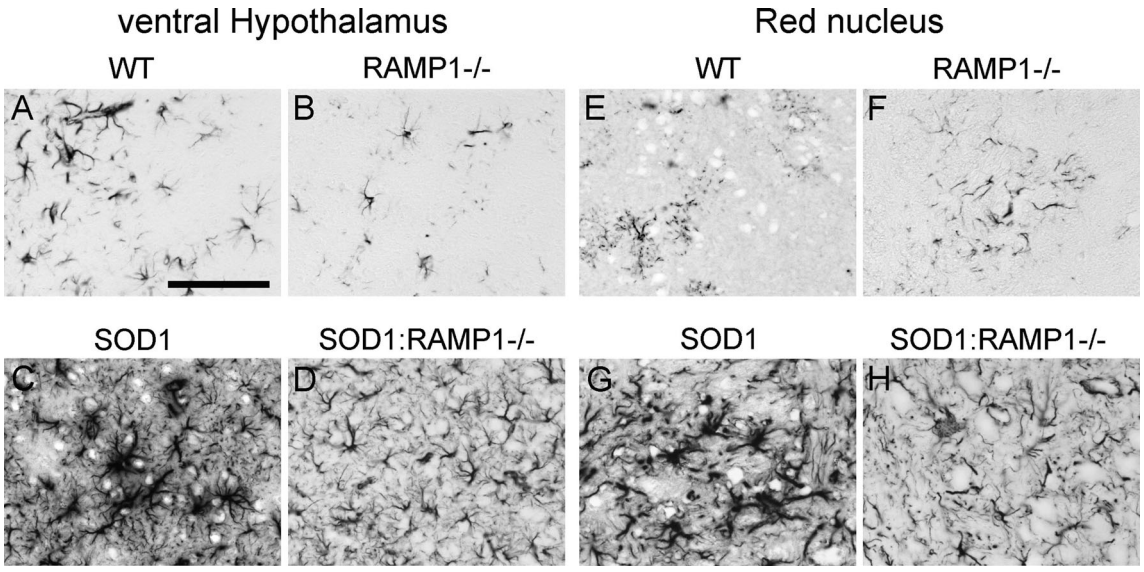

Fig. 4 Qualitative morphological assessment of astrogliosis in motor and non-motor brain regions. Both in the ventral hypothalamus (**a**–**d**) and in the red nucleus (**e**–**h**), the massive increase in GFAP-immunoreactive area seen in SOD1 mice at disease end stage (**c** + **g**) when compared with age-matched WT (**a** + **e**) and RAMP1−/− mice (**b** + **f**) is dampened in SOD1:RAMP1 knockout mice (**d** + **h**). The *bar* in **a** equals 100 µm and accounts for all pictures

end stage at P120 in SOD1:RAMP1−/− mice (Fig. 3d). At P120, both microgliosis and T-cell infiltration were largely reduced in SOD1:RAMP1−/− compared with SOD1:RAMP1+/+ (microglia: 112.7 ± 6.7 cells/mm^2 in SOD1:RAMP1+/+ vs. 86.6 ± 6.0 cells/mm^2 in SOD1:RAMP1−/−, $p < 0.001$; lymphocytes: 21.0 ± 1.5 cells/mm^2 in SOD1:RAMP1+/+ vs. 6.3 ± 0.8 cells/mm^2 in SOD1:RAMP1−/−; $p < 0.05$).

The RAMP1 deficiency alters the expression of neurotrophic factors and key inflammatory chemokines in SOD1 mice

To assess if the observed reductions in the morphological activation states of glia were accompanied by gene expression changes of neurotrophic factors and inflammatory chemokines that may depend on CGRP signaling, we investigated brain stem tissue from 3 to 5 SOD1:RAMP1+/+ and SOD1:RAMP1−/− mice each at P60, P90, and P120, and 3 WT and RAMP−/− mice each at P60 as controls by semi-quantitative RT-PCR.

Regarding neurotrophic factors (Fig. 5a), expression of glial cell line-derived neurotrophic factor (GDNF) was found unchanged in end-stage SOD1 mice of both genotypes when compared with WT. Expression of vascular endothelial growth factor (VEGF) was reduced to 52 ± 22 % in end-stage SOD1:RAMP1+/+ mice when compared with WT (0.53 ± 0.08 fold vs. 1.01 ± 0.1 fold, $p < 0.05$), while no decrease was detected in SOD1:RAMP1−/− when compared with RAMP1−/− (0.77 ± 0.14 fold vs. 0.99 ± 0.03 fold, p = n.s.). Finally, brain-derived neurotrophic factor (BDNF) was found elevated in SOD1:RAMP1−/− mice compared with SOD1:RAMP1+/+ (2.02 ± 0.42 fold vs. 0.81 ± 0.15 fold, respectively, $p < 0.01$) at disease end stage. The expression level of insulin like growth factor 1 (IGF-1) was similar in SOD1:RAMP1+/+ and SOD1:RAMP1−/− animals in all stages investigated (data not shown).

CD68 (macrosialin), a microglia marker, was found reduced in end-stage SOD1:RAMP1−/− mice compared with SOD1:RAMP1+/+ mice (15.51 ± 2.91 fold vs. 22.71 ± 0.27 fold, $p < 0.01$) (Fig. 5b). No expression changes were found for the specific marker genes for alternatively activated, anti-inflammatory (M2) microglia, arginase 1 and Ym1, or for the specific marker for classically activated, pro-inflammatory (M1) microglia, inducible nitric oxide synthase (data not shown).

With respect to pro- and anti-inflammatory cytokines, the expression levels of transforming growth factor beta (TGFβ), tumor necrosis factor alpha (TNFα), and interleukin 1 beta (IL-1β) were all found reduced in SOD1:RAMP1−/− compared with SOD1:RAMP1+/+ at disease end stage (TGFβ: 3.5 ± 0.26 fold vs. 2.34 ± 0.56 fold, $p < 0.001$; TNFα: 12.1 ± 4.25 fold vs. 25.8 ± 8.8 fold, $p < 0.001$; IL-1β: 11.83 ± 3.7 fold vs. 17.1 ± 25.6 fold, $p < 0.05$; Fig. 5c). In contrast, expression of interleukin 6 (IL-6) was enhanced in SOD1:RAMP1−/− end-stage mice only (5.6 ± 1.9 fold compared with WT: $p < 0.05$) while unaltered in SOD1:RAMP1+/+ (1.79 ± 1.9 fold; compared with WT, $p < 0.05$).

Since we found lymphocyte infiltration largely reduced in SOD1:RAMP1−/− mice, we also analyzed the yet unknown expression profiles of several T-cell attracting C-X-C and C-C motive chemokine ligands (CXCL and CCL, respectively) [44–46] in SOD1 mice at pre- as well as early and late symptomatic disease stages (Fig. 5d). While no changes in expression could be detected at the pre-symptomatic phase at P60 for CXCL10, CCL2 (monocyte chemoattractant protein 1; MCP-1), CCL3 (macrophage inflammatory protein 1a; MIP-1a), CCL5 (regulated on activation, normal T cell expressed and secreted; RANTES), and CCL8 (MCP-2, not shown), their expression was similarly elevated about 3–30-fold in end-stage mice ($p < 0.01$ for CXCL10 and CCL8; $p < 0.001$ for CCL2, CCL3, and CCL5). However, no differences in chemokine expression levels were detected between SOD1:RAMP1+/+ and SOD1:RAMP1−/− mice at any time point investigated.

Discussion

Involvement of CGRP in muscle denervation during ALS pathology

CGRP is synthesized by many, but not all motor neurons [34, 47, 48], and accumulates in the pre-synaptic NMJ [49, 50], where it is co-released with acetylcholine (ACh) in an action potential-dependent manner [51–53]. Subsequently, CGRP upregulates the ACh receptor [54–57] and the associated collagen ColQ [58] in the post-synaptic NMJ, and, therefore, has been implicated in the developmental formation of the NMJ [57, 59, 60]. While it has already been shown that αCGRP-deficient mice do not exhibit any disturbances in neuromuscular development [61] and motor performance [33], we now show for the first time that neither mice deficient in βCGRP (Fig. 2C) nor RAMP1 (Fig. 3a), with CGRP signaling fully eliminated in the latter, exert any deficits in hind limb grip endurance, fore limb grip strength (data not shown), and licking frequency. Thus, CGRP signaling is not essential for the development and the maintenance of the neuromuscular end plate and motor function under physiological conditions.

Our finding that muscle denervation in SOD1:RAMP1−/− mice precedes muscle denervation in

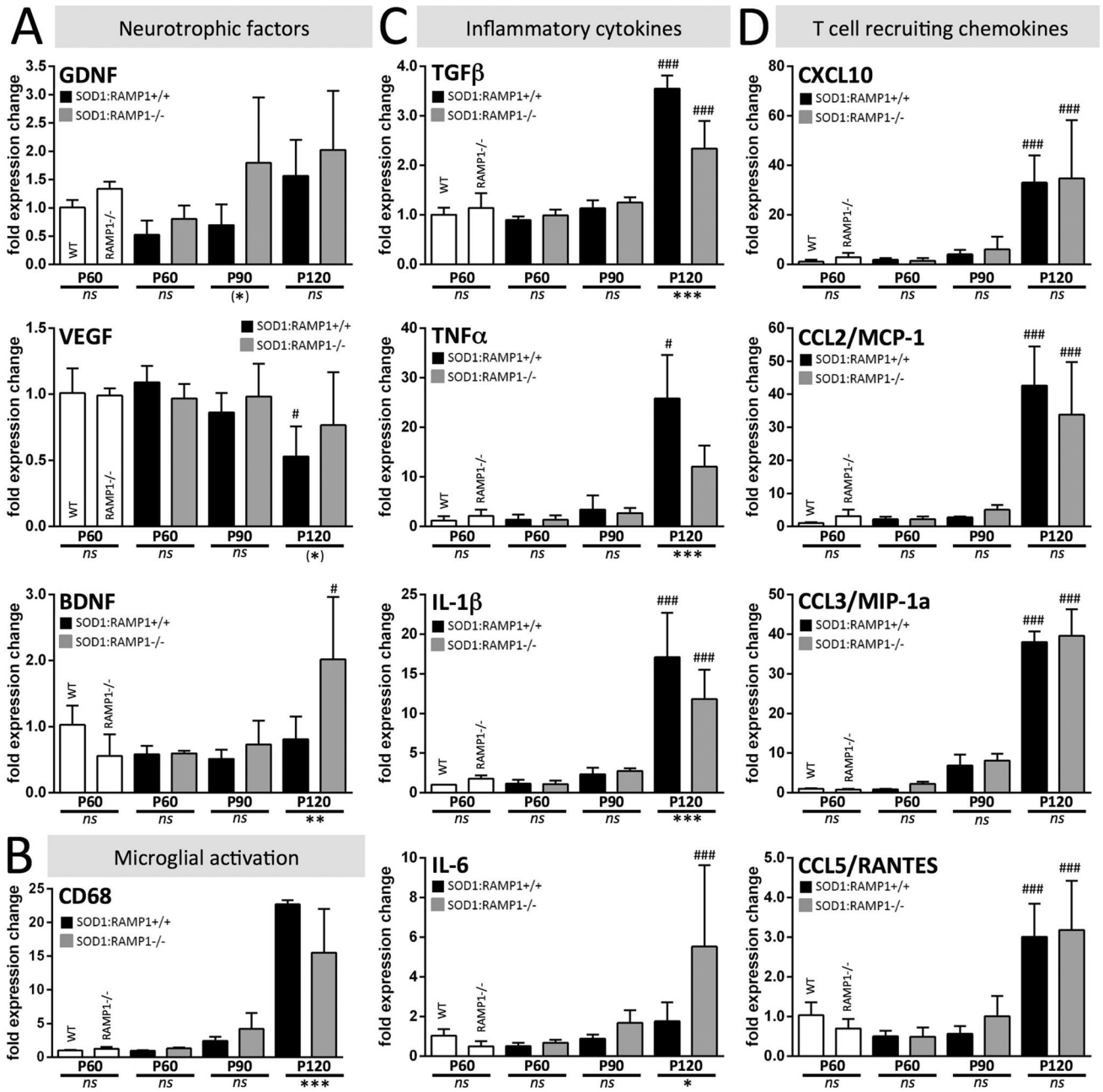

Fig. 5 Gene expression analysis in SOD1 brain stem tissue across disease stages. Real-time semi-quantitative RT-PCR was performed for 3–5 mice per genotype each at age P60, P90, and P120. Shown are the relative expression levels normalized to the geomean of *Actb* and *Ywhaz* (expression level %HC), and relative to WT (fold expression change). Group means were plotted ± SEM. $*p < 0.05$, $**p < 0.01$, $***p < 0.001$ (within the same age), $\#p < 0.05$ and $\#\#\#p < 0.001$ (compared with WT)

SOD1:RAMP1+/+ mice without any differences in motor neuron degeneration (Fig. 3c) implies a CGRP-dependent mechanism that allows the harmed motor neurons to maintain the NMJ until severe damage occurs (Fig. 6). A likely option is trophic support mediated via GDNF, the most potent neurotrophic factor for motor neurons [62–66]. A recent study showed that CGRP enhances GDNF secretion by myotubes in vitro [67], while GDNF delivery increased the number of CGRP-immunoreactive motor neurons in vivo [68, 69]. These findings suggest a reciprocal interaction between motor neuron-derived CGRP and muscle-derived GDNF that are essential for the maintenance of the NMJ in the early stages of motor neuron degeneration (Fig. 6). Accordingly, we hypothesize that the interruption of these interactions by RAMP1 depletion is accountable for the accelerated denervation and associated earlier symptom onset in SOD1:RAMP1−/− mice. Notably, a decrease in expression of muscle-derived GDNF

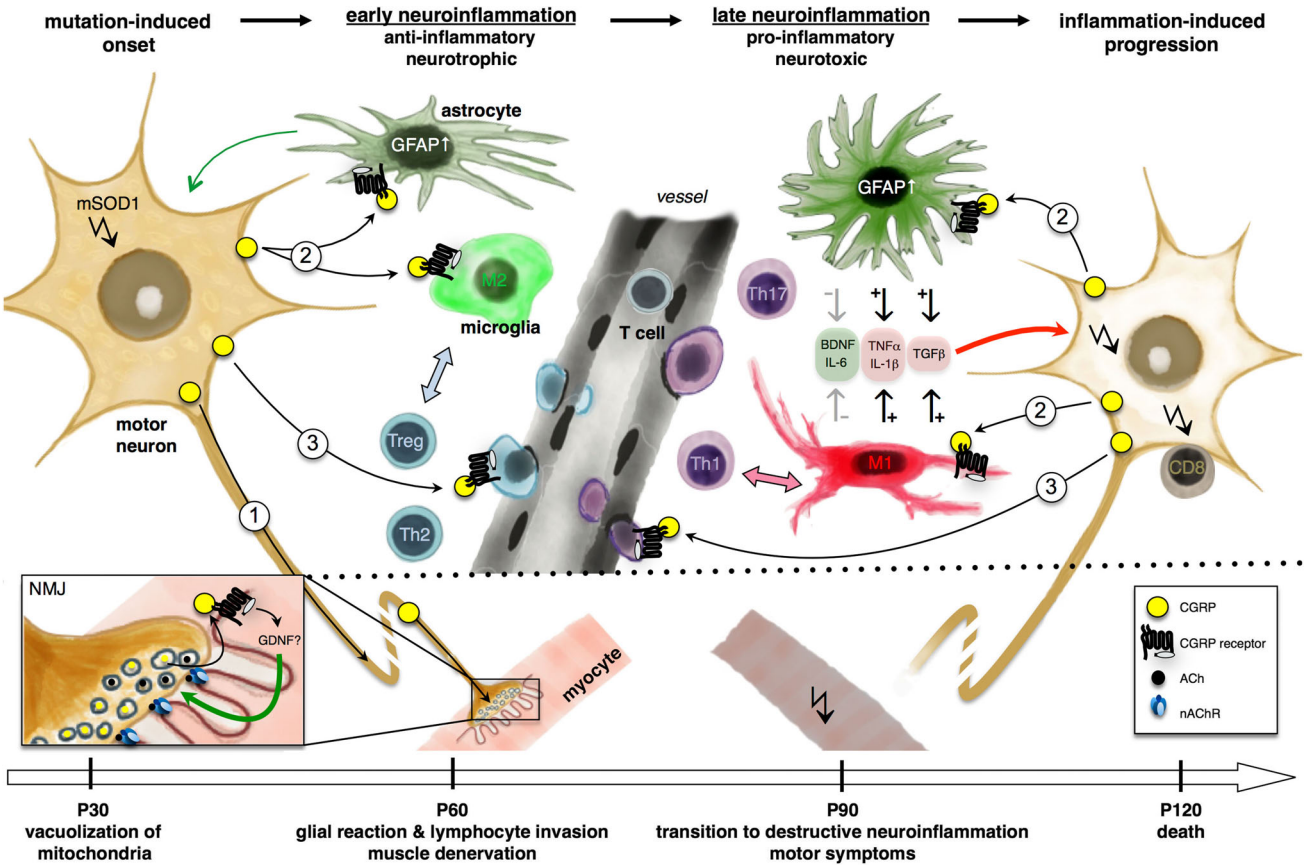

Fig. 6 Pathophysiological relevance of CGRP signaling in ALS. *1* While mutant SOD1 triggers motor neuron degeneration, a reciprocal interaction between motor neuron-derived CGRP and muscle-derived GDNF may be important for the maintenance of the NMJ in the early stages of motor neuron degeneration. An interruption of this interaction by a RAMP1 depletion accounts for the accelerated muscle denervation and the earlier symptom onset in SOD1:RAMP1−/− mice. *2* From early symptomatic stages onward, the degree of astrogliosis correlates with the abundance of CGRP, and an anti-inflammatory microglia activation state (M2) may be supported by CGRP (early neuroinflammation). During late-disease stages, continuous CGRP signaling leads to an enhancement of neurotoxic (TGFβ, TNFα, IL-1β) gene expression and dampened neurotrophic (BDNF) and anti-inflammatory (Il-6) gene expression in astrocytes and microglia (late neuroinflammation). Both glia reactions are reduced on the morphological level in SOD1:RAMP1−/− mice, with accompanying elevations or reductions in gene expression levels of neurotrophic, anti- and pro-inflammatory factors, respectively. *3* CGRP signaling onto lymphocytes is chemoattractant and promotes their infiltration into the brain parenchyma, both in early and in late-disease stages. A lymphocyte subtype change from Th2/Treg to Th1/Th17/CD8+ occurs during disease progression, analog to the switch of the anti-inflammatory microglia phenotype (M2) to a pro-inflammatory one (M1). The reduced recruitment of lymphocytes at late-disease stages in SOD1:RAMP1−/− mice, thus may prevent a disease-promoting interaction with neurotoxic microglia

at early disease stages most likely is functionally independent of the increase of GDNF expression that we found in the brain stem of SOD1:RAMP1−/− mice at later disease stages (see below).

Involvement of CGRP in neuroinflammation during ALS pathogenesis

A common characteristic that ALS shares with other neurodegenerative diseases is the occurrence of neuroinflammation, i.e., the activation of astrocytes and microglia [70, 71]. Both cell types express the CGRP-specific receptor complex [32, 72–75], and CGRP signaling on astrocytes and microglia in culture leads to the induction of c-fos followed by an upregulation of the activation marker GFAP and OX-42, respectively [30, 31, 76]. This is in line with our findings that in SOD1 mice, the degree of astrogliosis in affected brain regions was positively correlated with the abundance of CGRP in this region throughout the investigated disease stages (Fig. 1B), and that astrocyte and microglia activations on the morphological levels were largely reduced in SOD1:RAMP1−/− mice in most stages investigated (Fig. 3d).

Remarkably, neuroinflammation in ALS proceeds in two phases [15, 77–80]: In the early, pre-symptomatic disease stage, signals from damaged neurons induce

neuroprotective glia activation that is characterized by alternatively activated microglia (M2) secreting anti-inflammatory cytokines and neurotrophic factors that aid recovery. In contrast, when the neuroinflammation becomes chronic, the milieu switches to a neurodestructive phenotype characterized by classically activated microglia (M1) secreting pro-inflammatory cytokines and reactive oxygen species (ROS) that harm neighboring astrocytes and neurons. These mechanisms are thought to be the main drivers of the progression of motor neuron degeneration and, consequently, symptom development [81–83], and may lead to a progressive instability of the dynamic balance between pro- and anti-inflammatory chemokines [84]. Thus, our findings imply that CGRP induces and/or promotes cytotoxic neuroinflammation (Fig. 6).

This view is supported by our finding that the expression levels of two key pro-inflammatory chemokines, IL-1β and TNFα—the latter also known to exert direct toxic effects on motor neurons in vitro and in ALS mice [85–88]—were reduced in SOD1:RAMP1−/− end-stage animals (Fig. 5c). On the other hand, TGFβ, an anti-inflammatory cytokine that is considered to induce neuroprotective components of neuroinflammation in ALS [89], was reduced in SOD1:RAMP1−/− mice, while IL-6, that is suggested as pro-inflammatory cytokine in ALS-related neuroinflammation [83, 90, 91], was elevated. However, a recent study showed that overexpression of TGFβ accelerated disease progression, while treatment with a TGFβ antagonist extended the lifespan in SOD1 mice [92]. This is in line with our finding of reduced TGFβ expression and decelerated disease progression in SOD1:RAMP1−/− mice. Likewise, IL-6 is a multifunctional chemokine [90] that improves neuronal survival following axotomy, oxidative stress, and excitotoxicity, and may, therefore, positively modulate central pathomechanisms in ALS in vivo and in vitro [93, 94], especially in the presence of BDNF [95] which we found elevated on the mRNA level in SOD1:RAMP1−/− compared with SOD1:RAMP1+/+ mice at end stage. Similarly, GDNF and VEGF mRNA expression levels were slightly higher in SOD1:RAMP1−/− compared with SOD1:RAMP1+/+ mice at P90 and at disease end stage, respectively, indicating that at later disease stages, the central neurotrophic support delivered by glia cells was generally stronger in SOD1:RAMP1−/− mice.

Taken together and in light of the decelerated disease progression found in SOD1:RAMP1−/− mice, we consider the reduction in glial activation and the changes of the cytokine expression patterns in the late-stage SOD1:RAMP1−/− mice as beneficial, and hypothesize, in turn, that CGRP promotes the neurotoxic features of the neuroinflammation at the late disease stages (Fig. 6).

Involvement of CGRP in T-cell recruitment during ALS pathogenesis

Besides the activation of astro- and microglia, the infiltration of T-lymphocytes is another hallmark of ALS-related neuroinflammation [15, 77–80]. In the early disease stages, regulatory T cells (Treg) and T helper type 2 cells (Th2) exert anti-inflammatory effects that delay symptom onset [15, 96], whereas in later disease stages, Th1 and Th17 cells as well as cytotoxic T cells (CD8 +) contribute to the cytotoxic inflammatory milieu and motor neuron degeneration. All T-cell subsets express the CGRP-specific receptor complex [72, 97], and CGRP functions as a potent chemoattractant for lymphocytes [98–100]. This might explain why we found lymphocyte infiltration largely reduced in SOD1:RAMP1−/− mice (Fig. 3d), even though the expression of none of the key chemokines was altered compared with SOD1:RAMP1+/+ mice (Fig. 5d). In line with their contribution to the inflammatory milieu, the reduction of anti-inflammatory and regulatory T-cell subtypes in the early disease stages might contribute to the accelerated symptom onset. On the other hand, the reduction in pro-inflammatory and cytotoxic T-cell subsets in the late disease stages might contribute to the decelerated disease progression in SOD1:RAMP1−/− mice (Fig. 6).

Considering that RAMP1−/− mice are resistant to the induction of experimental autoimmune encephalomyelitis due to the absence of T-cell infiltration [101], we conclude that CGRP is an essential factor for the recruitment of T cells to the CNS in ALS.

In addition, IL-6 aids to maintain the integrity of the blood–brain barrier by antagonizing TNFα- and IL-1β-mediated regulation of integrin expression in astrocytes [102–104]. Consequently, our results that TNFα and IL-1β expression levels are reduced while IL-6 is elevated suggest that the blood–brain barrier might be largely unharmed in the late-stage SOD1:RAMP1−/− mice which might impede T-cell infiltration as well.

Involvement of additional RAMP1-mediated pathways

It has been shown in vitro that RAMP1 can also bind to the calcium-sensing receptor (CaSR) [105, 106] and the vasoactive intestinal peptide/pituitary adenylate cyclase-activating peptide 1 receptor (VPAC1) [107] and facilitate their shuttling to the cell surface. CaSR seems to be an essential protein for the organism, because CaSR knockout mice die prematurely due to metabolic problems [108]. If the RAMP1 proteins were essentially required for trafficking of the CaSR to the cell surface, a RAMP1 deficiency should prevent this trafficking and ultimately result in the same lethal phenotype, which is not the case

([36], this study). Similarly, the association of RAMP1 with VPAC1 found in vitro [107, 109] is not an obligatory relationship [105] and a validation in vivo still needs to be shown. Thus, we conclude that the RAMP1 deficiency should not interfere with the function of the aforementioned receptors and that the RAMP1 phenotype we observe in our study using the mutant SOD1 mouse resulted from a CGRP signaling deficit only.

Conclusion

CGRP signaling through the RAMP1/CLR/RCP receptor complex may serve a dual role in ALS pathogenesis. Pharmacological or immunological targeting of panCGRP, or of the CGRP receptor complex in future experiments should be pursued, as long as treatment direction (agonism vs. antagonism) and disease stage (early vs. late) are properly controlled for.

Acknowledgments We are grateful to Carola Gäckler, Michael Schneider, and Marion Zibuschka for excellent technical assistance. This work was supported by funds from the University Medical Center Giessen and Marburg (UKGM), by the P. E. Kempkes Foundation (University of Marburg), and by grants from the German Society for the Muscular Diseased (DGM, Freiburg, Germany).

Compliance with ethical standards

Conflict of interest The authors declare that they have no conflict of interest.

References

1. Sendtner M (2014) Motoneuron disease. Handb Exp Pharmacol 220:411–441. doi:10.1007/978-3-642-45106-5_15
2. Kiernan MC, Vucic S, Cheah BC et al (2011) Amyotrophic lateral sclerosis. Lancet 377:942–955. doi:10.1016/S0140-6736(10)61156-7
3. Sreedharan J, Brown RHJ (2013) Amyotrophic lateral sclerosis: Problems and prospects. Ann Neurol 74:309–316. doi:10.1002/ana.24012
4. Van Langenhove T, van der Zee J, Van Broeckhoven C (2012) The molecular basis of the frontotemporal lobar degeneration-amyotrophic lateral sclerosis spectrum. Ann Med 44:817–828. doi:10.3109/07853890.2012.665471
5. Kato S (2008) Amyotrophic lateral sclerosis models and human neuropathology: similarities and differences. Acta Neuropathol 115:97–114. doi:10.1007/s00401-007-0308-4
6. Philips T, Rothstein JD (2015) Rodent models of amyotrophic lateral sclerosis. Curr Protoc Pharmacol 69:5.67.1–5.67.21. doi:10.1002/0471141755.ph0567s69
7. Gurney ME (1994) Transgenic-mouse model of amyotrophic lateral sclerosis. N Engl J Med 331:1721–1722. doi:10.1056/NEJM199412223312516
8. Kong J, Xu Z (1998) Massive mitochondrial degeneration in motor neurons triggers the onset of amyotrophic lateral sclerosis in mice expressing a mutant SOD1. J Neurosci 18:3241–3250
9. Jaarsma D, Haasdijk ED, Grashorn JA et al (2000) Human Cu/Zn superoxide dismutase (SOD1) overexpression in mice causes mitochondrial vacuolization, axonal degeneration, and premature motoneuron death and accelerates motoneuron disease in mice expressing a familial amyotrophic lateral sclerosis mutant SOD1. Neurobiol Dis 7:623–643. doi:10.1006/nbdi.2000.0299
10. Fischer LR, Culver DG, Tennant P et al (2004) Amyotrophic lateral sclerosis is a distal axonopathy: evidence in mice and man. Exp Neurol 185:232–240
11. Pun S, Santos AF, Saxena S et al (2006) Selective vulnerability and pruning of phasic motoneuron axons in motoneuron disease alleviated by CNTF. Nat Neurosci 9:408–419. doi:10.1038/nn1653
12. Hall ED, Oostveen JA, Gurney ME (1998) Relationship of microglial and astrocytic activation to disease onset and progression in a transgenic model of familial ALS. Glia 23:249–256. doi:10.1002/(SICI)1098-1136(199807)23:3<249:AID-GLIA7>3.0.CO;2-#
13. Barbeito LH, Pehar M, Cassina P et al (2004) A role for astrocytes in motor neuron loss in amyotrophic lateral sclerosis. Brain Res Rev 47:263–274. doi:10.1016/j.brainresrev.2004.05.003
14. Graves MC, Fiala M, Dinglasan LAV et al (2004) Inflammation in amyotrophic lateral sclerosis spinal cord and brain is mediated by activated macrophages, mast cells and T cells. Amyotroph Lateral Scler Other Motor Neuron Disord 5:213–219
15. Beers DR, Henkel JS, Zhao W et al (2008) CD4 + T cells support glial neuroprotection, slow disease progression, and modify glial morphology in an animal model of inherited ALS. Proc Natl Acad Sci USA 105:15558–15563. doi:10.1073/pnas.0807419105
16. Schutz B, Reimann J, Dumitrescu-Ozimek L et al (2005) The oral antidiabetic pioglitazone protects from neurodegeneration and amyotrophic lateral sclerosis-like symptoms in superoxide dismutase-G93A transgenic mice. J Neurosci 25:7805–7812. doi:10.1523/JNEUROSCI.2038-05.2005
17. Wimalawansa SJ (1996) Calcitonin gene-related peptide and its receptors: molecular genetics, physiology, pathophysiology, and therapeutic potentials. Endocr Rev 17:533–585
18. van Rossum D, Hanisch UK, Quirion R (1997) Neuroanatomical localization, pharmacological characterization and functions of CGRP, related peptides and their receptors. Neurosci Biobehav Rev 21:649–678
19. Evans BN, Rosenblatt MI, Mnayer LO et al (2000) CGRP-RCP, a novel protein required for signal transduction at calcitonin gene-related peptide and adrenomedullin receptors. J Biol Chem 275:31438–31443. doi:10.1074/jbc.M005604200
20. Walker CS, Conner AC, Poyner DR, Hay DL (2010) Regulation of signal transduction by calcitonin gene-related peptide receptors. Trends Pharmacol Sci 31:476–483. doi:10.1016/j.tips.2010.06.006
21. McLatchie LM, Fraser NJ, Main MJ et al (1998) RAMPs regulate the transport and ligand specificity of the calcitonin-receptor-like receptor. Nature 393:333–339. doi:10.1038/30666
22. Moreno MJ, Terron JA, Stanimirovic DB et al (2002) Characterization of calcitonin gene-related peptide (CGRP) receptors and their receptor-activity-modifying proteins (RAMPs) in human brain microvascular and astroglial cells in culture. Neuropharmacology 42:270–280
23. Wang Z, Ma W, Chabot J-G, Quirion R (2010) Morphological evidence for the involvement of microglial p38 activation in CGRP-associated development of morphine antinociceptive tolerance. Peptides 31:2179–2184. doi:10.1016/j.peptides.2010.08.020

24. Fukuoka T, Tokunaga A, Kondo E et al (1999) Differential regulation of alpha- and beta-CGRP mRNAs within oculomotor, trochlear, abducens, and trigeminal motoneurons in response to axotomy. Brain Res Mol Brain Res 63:304–315
25. Nohr D, Schafer MK, Persson S et al (1999) Calcitonin gene-related peptide gene expression in collagen-induced arthritis is differentially regulated in primary afferents and motoneurons: influence of glucocorticoids. Neuroscience 93:759–773
26. Weihe E, Nohr D, Schafer MK et al (1995) Calcitonin gene related peptide gene expression in collagen-induced arthritis. Can J Physiol Pharmacol 73:1015–1019
27. Rohrenbeck AM, Bette M, Hooper DC et al (1999) Upregulation of COX-2 and CGRP expression in resident cells of the Borna disease virus-infected brain is dependent upon inflammation. Neurobiol Dis 6:15–34. doi:10.1006/nbdi.1998.0225
28. Weihe E, Bette M, Preuss MA et al (2008) Role of virus-induced neuropeptides in the brain in the pathogenesis of rabies. Dev Biol (Basel) 131:73–81
29. Morara S, Wang L-P, Filippov V et al (2008) Calcitonin gene-related peptide (CGRP) triggers Ca^{2+} responses in cultured astrocytes and in Bergmann glial cells from cerebellar slices. Eur J Neurosci 28:2213–2220. doi:10.1111/j.1460-9568.2008.06514.x
30. Priller J, Haas CA, Reddington M, Kreutzberg GW (1995) Calcitonin gene-related peptide and ATP induce immediate early gene expression in cultured rat microglial cells. Glia 15:447–457. doi:10.1002/glia.440150408
31. Haas CA, Reddington M, Kreutzberg GW (1991) Calcitonin gene-related peptide stimulates the induction of c-fos gene expression in rat astrocyte cultures. Eur J Neurosci 3:708–712
32. Reddington M, Priller J, Treichel J et al (1995) Astrocytes and microglia as potential targets for calcitonin gene related peptide in the central nervous system. Can J Physiol Pharmacol 73:1047–1049
33. Ringer C, Weihe E, Schutz B (2009) Pre-symptomatic alterations in subcellular betaCGRP distribution in motor neurons precede astrogliosis in ALS mice. Neurobiol Dis 35:286–295. doi:10.1016/j.nbd.2009.05.011
34. Ringer C, Weihe E, Schutz B (2012) Calcitonin gene-related peptide expression levels predict motor neuron vulnerability in the superoxide dismutase 1-G93A mouse model of amyotrophic lateral sclerosis. Neurobiol Dis 45:547–554. doi:10.1016/j.nbd.2011.09.011
35. Gurney ME, Pu H, Chiu AY et al (1994) Motor neuron degeneration in mice that express a human Cu, Zn superoxide dismutase mutation. Science 264:1772–1775
36. Tsujikawa K, Yayama K, Hayashi T et al (2007) Hypertension and dysregulated proinflammatory cytokine production in receptor activity-modifying protein 1-deficient mice. Proc Natl Acad Sci USA 104:16702–16707. doi:10.1073/pnas.0705974104
37. Weydt P, Hong SY, Kliot M, Moller T (2003) Assessing disease onset and progression in the SOD1 mouse model of ALS. Neuroreport 14:1051–1054. doi:10.1097/01.wnr.0000073685.00308.89
38. Hayar A, Bryant JL, Boughter JD, Heck DH (2006) A low-cost solution to measure mouse licking in an electrophysiological setup with a standard analog-to-digital converter. J Neurosci Methods 153:203–207. doi:10.1016/j.jneumeth.2005.10.023
39. Fuchs A, Ringer C, Bilkei-Gorzo A et al (2010) Downregulation of the potassium chloride cotransporter KCC2 in vulnerable motoneurons in the SOD1-G93A mouse model of amyotrophic lateral sclerosis. J Neuropathol Exp Neurol 69:1057–1070. doi:10.1097/NEN.0b013e3181f4dcef
40. Schutz B, Chen L, Schafer MK et al (2000) Somatomotor neuron-specific expression of the human cholinergic gene locus in transgenic mice. Neuroscience 96:707–722
41. Ringer C, Buning LS, Schafer MK et al (2013) PACAP signaling exerts opposing effects on neuroprotection and neuroinflammation during disease progression in the SOD1 (G93A) mouse model of amyotrophic lateral sclerosis. Neurobiol Dis 54C:32–42. doi:10.1016/j.nbd.2013.02.010
42. Jaarsma D, Rognoni F, van Duijn W et al (2001) CuZn superoxide dismutase (SOD1) accumulates in vacuolated mitochondria in transgenic mice expressing amyotrophic lateral sclerosis-linked SOD1 mutations. Acta Neuropathol 102:293–305
43. Leichsenring A, Linnartz B, Zhu XR et al (2006) Ascending neuropathology in the CNS of a mutant SOD1 mouse model of amyotrophic lateral sclerosis. Brain Res 1096:180–195. doi:10.1016/j.brainres.2006.04.029
44. Taub DD, Oppenheim JJ (1994) Chemokines, inflammation and the immune system. Ther Immunol 1:229–246
45. Ward SG, Westwick J (1998) Chemokines: understanding their role in T-lymphocyte biology. Biochem J 333(Pt 3):457–470
46. Ward SG, Bacon K, Westwick J (1998) Chemokines and T lymphocytes: more than an attraction. Immunity 9:1–11
47. Arvidsson U, Piehl F, Johnson H et al (1993) The peptidergic motoneurone. Neuroreport 4:849–856
48. Behzadi G, Ganji F (2005) Morphological alteration in oro-facial CGRP containing motoneurons due to congenital thyroid hypofunction. Peptides 26:1486–1491. doi:10.1016/j.peptides.2005.03.053
49. Mora M, Marchi M, Polak JM et al (1989) Calcitonin gene-related peptide immunoreactivity at the human neuromuscular junction. Brain Res 492:404–407
50. Choi RC, Yung LY, Dong TT et al (1998) The calcitonin gene-related peptide-induced acetylcholinesterase synthesis in cultured chick myotubes is mediated by cyclic AMP. J Neurochem 71:152–160
51. Uchida S, Yamamoto H, Iio S et al (1990) Release of calcitonin gene-related peptide-like immunoreactive substance from neuromuscular junction by nerve excitation and its action on striated muscle. J Neurochem 54:1000–1003
52. Sakaguchi M, Inaishi Y, Kashihara Y, Kuno M (1991) Release of calcitonin gene-related peptide from nerve terminals in rat skeletal muscle. J Physiol 434:257–270
53. Sala C, Andreose JS, Fumagalli G, Lømo T (1995) Calcitonin gene-related peptide: possible role in formation and maintenance of neuromuscular junctions. J Neurosci 15:520–528
54. New HV, Mudge AW (1986) Calcitonin gene-related peptide regulates muscle acetylcholine receptor synthesis. Nature 323:809–811. doi:10.1038/323809a0
55. Fontaine B, Klarsfeld A, Changeux JP (1987) Calcitonin gene-related peptide and muscle activity regulate acetylcholine receptor alpha-subunit mRNA levels by distinct intracellular pathways. J Cell Biol 105:1337–1342
56. da Costa VL, Lapa AJ, Godinho RO (2001) Short- and long-term influences of calcitonin gene-related peptide on the synthesis of acetylcholinesterase in mammalian myotubes. Br J Pharmacol 133:229–236. doi:10.1038/sj.bjp.0704069
57. Buffelli M, Pasino E, Cangiano A (2001) In vivo acetylcholine receptor expression induced by calcitonin gene-related peptide in rat soleus muscle. Neuroscience 104:561–567
58. Choi RC, Ting AK, Lau FT et al (2007) Calcitonin gene-related peptide induces the expression of acetylcholinesterase-associated collagen ColQ in muscle: a distinction in driving two different promoters between fast- and slow-twitch muscle fibers. J Neurochem 102:1316–1328. doi:10.1111/j.1471-4159.2007.4630.x
59. Fontaine B, Klarsfeld A, Hokfelt T, Changeux JP (1986) Calcitonin gene-related peptide, a peptide present in spinal cord motoneurons, increases the number of acetylcholine receptors in

primary cultures of chick embryo myotubes. Neurosci Lett 71:59–65
60. Daniels MP (1997) Intercellular communication that mediates formation of the neuromuscular junction. Mol Neurobiol 14:143–170. doi:10.1007/BF02740654
61. Lu JT, Son YJ, Lee J et al (1999) Mice lacking alpha-calcitonin gene-related peptide exhibit normal cardiovascular regulation and neuromuscular development. Mol Cell Neurosci 14:99–120. doi:10.1006/mcne.1999.0767
62. Henderson CE, Phillips HS, Pollock RA et al (1994) GDNF: a potent survival factor for motoneurons present in peripheral nerve and muscle. Science 266:1062–1064
63. Zurn AD, Baetge EE, Hammang JP et al (1994) Glial cell line-derived neurotrophic factor (GDNF), a new neurotrophic factor for motoneurones. Neuroreport 6:113–118
64. Oppenheim RW, Houenou LJ, Johnson JE et al (1995) Developing motor neurons rescued from programmed and axotomy-induced cell death by GDNF. Nature 373:344–346. doi:10.1038/373344a0
65. Yan Q, Matheson C, Lopez OT (1995) In vivo neurotrophic effects of GDNF on neonatal and adult facial motor neurons. Nature 373:341–344. doi:10.1038/373341a0
66. Hottinger AF, Azzouz M, Déglon N et al (2000) Complete and long-term rescue of lesioned adult motoneurons by lentiviral-mediated expression of glial cell line-derived neurotrophic factor in the facial nucleus. J Neurosci 20:5587–5593
67. Rosa E, Cha J, Bain JR, Fahnestock M (2015) Calcitonin gene-related peptide regulation of glial cell-line derived neurotrophic factor in differentiated rat myotubes. J Neurosci Res 93:514–520. doi:10.1002/jnr.23512
68. Ramer MS, Bradbury EJ, Michael GJ et al (2003) Glial cell line-derived neurotrophic factor increases calcitonin gene-related peptide immunoreactivity in sensory and motoneurons in vivo. Eur J Neurosci 18:2713–2721
69. Blesch A, Tuszynski MH (2001) GDNF gene delivery to injured adult CNS motor neurons promotes axonal growth, expression of the trophic neuropeptide CGRP, and cellular protection. J Comp Neurol 436:399–410
70. Glass CK, Saijo K, Winner B et al (2010) Mechanisms underlying inflammation in neurodegeneration. Cell 140:918–934. doi:10.1016/j.cell.2010.02.016
71. Appel SH, Beers DR, Henkel JS (2010) T cell-microglial dialogue in Parkinson's disease and amyotrophic lateral sclerosis: are we listening? Trends Immunol 31:7–17. doi:10.1016/j.it.2009.09.003
72. Umeda Y, Arisawa M (1989) Characterization of the calcitonin gene-related peptide receptor in mouse T lymphocytes. Neuropeptides 14:237–242
73. Morara S, Wimalawansa SJ, Rosina A (1998) Monoclonal antibodies reveal expression of the CGRP receptor in Purkinje cells, interneurons and astrocytes of rat cerebellar cortex. Neuroreport 9:3755–3759
74. De Corato A, Lisi L, Capuano A et al (2011) Trigeminal satellite cells express functional calcitonin gene-related peptide receptors, whose activation enhances interleukin-1β pro-inflammatory effects. J Neuroimmunol 237:39–46. doi:10.1016/j.jneuroim.2011.05.013
75. Consonni A, Morara S, Codazzi F et al (2011) Inhibition of lipopolysaccharide-induced microglia activation by calcitonin gene related peptide and adrenomedullin. Mol Cell Neurosci. doi:10.1016/j.mcn.2011.07.006
76. Cady RJ, Glenn JR, Smith KM, Durham PL (2011) Calcitonin gene-related peptide promotes cellular changes in trigeminal neurons and glia implicated in peripheral and central sensitization. Mol Pain 7:94. doi:10.1186/1744-8069-7-94
77. Streit WJ, Xue QS (2009) Life and death of microglia. J Neuroimmune Pharmacol: Off J Soc Neuroimmune Pharmacol 4:371–379. doi:10.1007/s11481-009-9163-5
78. Liao B, Zhao W, Beers DR et al (2012) Transformation from a neuroprotective to a neurotoxic microglial phenotype in a mouse model of ALS. Exp Neurol 237:147–152. doi:10.1016/j.expneurol.2012.06.011
79. Philips T, Robberecht W (2011) Neuroinflammation in amyotrophic lateral sclerosis: role of glial activation in motor neuron disease. Lancet Neurol 10:253–263. doi:10.1016/S1474-4422(11)70015-1
80. Henkel JS, Beers DR, Zhao W, Appel SH (2009) Microglia in ALS: the good, the bad, and the resting. J Neuroimmune Pharmacol: Off J Soc NeuroImmune Pharmacol 4:389–398. doi:10.1007/s11481-009-9171-5
81. Alexianu ME, Kozovska M, Appel SH (2001) Immune reactivity in a mouse model of familial ALS correlates with disease progression. Neurology 57:1282–1289
82. Boillee S, Vandevelde C, Cleveland D (2006) ALS: a disease of motor neurons and their nonneuronal neighbors. Neuron 52:39–59. doi:10.1016/j.neuron.2006.09.018
83. Zhao W, Beers DR, Appel SH (2013) Immune-mediated mechanisms in the pathoprogression of amyotrophic lateral sclerosis. J Neuroimmune Pharmacol: Off J Soc Neuroimmune Pharmacol 8:888–899. doi:10.1007/s11481-013-9489-x
84. Jeyachandran A, Mertens B, McKissick EA, Mitchell CS (2015) Type I vs. type II cytokine levels as a function of SOD1 G93A mouse amyotrophic lateral sclerosis disease progression. Front Cell Neurosci 9:462. doi:10.3389/fncel.2015.00462
85. Mir M, Asensio VJ, Tolosa L et al (2009) Tumor necrosis factor alpha and interferon gamma cooperatively induce oxidative stress and motoneuron death in rat spinal cord embryonic explants. Neuroscience 162:959–971. doi:10.1016/j.neuroscience.2009.05.049
86. Yin HZ, Hsu CI, Yu S et al (2012) TNF-alpha triggers rapid membrane insertion of Ca(2+) permeable AMPA receptors into adult motor neurons and enhances their susceptibility to slow excitotoxic injury. Exp Neurol 238:93–102. doi:10.1016/j.expneurol.2012.08.004
87. Tolosa L, Caraballo-Miralles V, Olmos G, Lladó J (2011) TNF-α potentiates glutamate-induced spinal cord motoneuron death via NF-κB. Mol Cell Neurosci 46:176–186. doi:10.1016/j.mcn.2010.09.001
88. Tortarolo M, Vallarola A, Lidonnici D et al (2015) Lack of TNF-alpha receptor type 2 protects motor neurons in a cellular model of amyotrophic lateral sclerosis and in mutant SOD1 mice but does not affect disease progression. J Neurochem. doi:10.1111/jnc.13154
89. Katsuno M, Adachi H, Banno H et al (2011) Transforming growth factor-β signaling in motor neuron diseases. Curr Mol Med 11:48–56
90. Spooren A, Kolmus K, Laureys G et al (2011) Interleukin-6, a mental cytokine. Brain Res Rev 67:157–183. doi:10.1016/j.brainresrev.2011.01.002
91. Evans MC, Couch Y, Sibson N, Turner MR (2013) Inflammation and neurovascular changes in amyotrophic lateral sclerosis. Mol Cell Neurosci 53:34–41. doi:10.1016/j.mcn.2012.10.008
92. Endo F, Komine O, Fujimori-Tonou N et al (2015) Astrocyte-derived TGF-β1 accelerates disease progression in ALS mice by interfering with the neuroprotective functions of microglia and T cells. Cell Rep 11:592–604. doi:10.1016/j.celrep.2015.03.053
93. Krady JK, Lin H-W, Liberto CM et al (2008) Ciliary neurotrophic factor and interleukin-6 differentially activate microglia. J Neurosci Res 86:1538–1547. doi:10.1002/jnr.21620
94. Eskes C, Honegger P, Juillerat-Jeanneret L, Monnet-Tschudi F (2002) Microglial reaction induced by noncytotoxic methylmercury treatment leads to neuroprotection via

interactions with astrocytes and IL-6 release. Glia 37:43–52. doi:10.1002/glia.10019
95. Murphy PG, Borthwick LA, Altares M et al (2000) Reciprocal actions of interleukin-6 and brain-derived neurotrophic factor on rat and mouse primary sensory neurons. Eur J Neurosci 12:1891–1899
96. Beers DR, Henkel JS, Zhao W et al (2011) Endogenous regulatory T lymphocytes ameliorate amyotrophic lateral sclerosis in mice and correlate with disease progression in patients with amyotrophic lateral sclerosis. Brain 134:1293–1314. doi:10.1093/brain/awr074
97. McGillis JP, Humphreys S, Reid S (1991) Characterization of functional calcitonin gene-related peptide receptors on rat lymphocytes. J Immunol 147:3482–3489
98. Foster CA, Mandak B, Kromer E, Rot A (1992) Calcitonin gene-related peptide is chemotactic for human T lymphocytes. Ann N Y Acad Sci 657:397–404
99. Talme T, Liu Z, Sundqvist K (2008) The neuropeptide calcitonin gene-related peptide (CGRP) stimulates T cell migration into collagen matrices. J Neuroimmunol 196:60–66. doi:10.1016/j.jneuroim.2008.02.007
100. Levite M (2000) Nerve-driven immunity. The direct effects of neurotransmitters on T-cell function. Ann N Y Acad Sci 917:307–321
101. Mikami N, Watanabe K, Hashimoto N et al (2012) Calcitonin gene-related peptide enhances experimental autoimmune encephalomyelitis by promoting Th17-cell functions. Int Immunol 24:681–691. doi:10.1093/intimm/dxs075
102. Oh JW, Van Wagoner NJ, Rose-John S, Benveniste EN (1998) Role of IL-6 and the soluble IL-6 receptor in inhibition of VCAM-1 gene expression. J Immunol 161:4992–4999
103. Rosenman SJ, Shrikant P, Dubb L et al (1995) Cytokine-induced expression of vascular cell adhesion molecule-1 (VCAM-1) by astrocytes and astrocytoma cell lines. J Immunol 154:1888–1899
104. Shrikant P, Weber E, Jilling T, Benveniste EN (1995) Intercellular adhesion molecule-1 gene expression by glial cells. Differential mechanisms of inhibition by IL-10 and IL-6. J Immunol 155:1489–1501
105. Desai AJ, Roberts DJ, Richards GO, Skerry TM (2014) Role of receptor activity modifying protein 1 in function of the calcium sensing receptor in the human TT thyroid carcinoma cell line. PLoS One 9:e85237. doi:10.1371/journal.pone.0085237
106. Bouschet T, Martin S, Henley JM (2005) Receptor-activity-modifying proteins are required for forward trafficking of the calcium-sensing receptor to the plasma membrane. J Cell Sci 118:4709–4720. doi:10.1242/jcs.02598
107. Christopoulos A, Christopoulos G, Morfis M et al (2003) Novel receptor partners and function of receptor activity-modifying proteins. J Biol Chem 278:3293–3297. doi:10.1074/jbc.C200629200
108. Ho C, Conner DA, Pollak MR et al (1995) A mouse model of human familial hypocalciuric hypercalcemia and neonatal severe hyperparathyroidism. Nat Genet 11:389–394. doi:10.1038/ng1295-389
109. Hay DL, Pioszak AA (2016) Receptor activity-modifying proteins (RAMPs): new insights and roles. Annu Rev Pharmacol Toxicol 56:469–487. doi:10.1146/annurev-pharmtox-010715-103120